

UNIVERSITY OF SOUTHAMPTON
Faculty of Engineering and Physical Sciences
School of Electronics and Computer Science

A project report submitted for the award of
BEng Electronic Engineering

Supervisor: Prof. S. Gunn
Examiner: Prof. M.C. Schraefel

**Development of a Cycling Club
Race Timing System.**

by **Jacob Burge**

April 24, 2019

UNIVERSITY OF SOUTHAMPTON

ABSTRACT

FACULTY OF ENGINEERING AND PHYSICAL SCIENCES
SCHOOL OF ELECTRONICS AND COMPUTER SCIENCE

A project report submitted for the award of BEng Electronic Engineering

Development of a Cycling Club Race Timing System.

by Jacob Burge

This project is intended to save cycling club race organisers from the labour intensive, time consuming and common practice of manual race result generation. While many electronic timing systems already exist, barriers to entry such as cost, operational complexity and general limitations make them only suitable for use by professional timing companies. With the aim of developing an alternative product that would enable club volunteers to generate results to a professional standard, while reducing the time required and process complexity, the system developed is considered a competitive solution. A system precision exceeding $\pm 10\text{ms}$ for 90% of detections is achieved while a minimum reliability of 99.7% for detections is observed. While existing systems advertise higher precision, the additional features of full waterproofing, user replaceable batteries and general ease of use at a significantly reduced price point, makes the system unique.

Statement of Originality

- I have read and understood the ECS Academic Integrity information and the University's Academic Integrity Guidance for Students.
- I am aware that failure to act in accordance with the Regulations Governing Academic Integrity may lead to the imposition of penalties which, for the most serious cases, may include termination of programme.
- I consent to the University copying and distributing any or all of my work in any form and using third parties (who may be based outside the EU/EEA) to verify whether my work contains plagiarised material, and for quality assurance purposes.

We expect you to acknowledge all sources of information (e.g. ideas, algorithms, data) using citations. You must also put quotation marks around any sections of text that you have copied without paraphrasing. If any figures or tables have been taken or modified from another source, you must explain this in the caption and cite the original source.

I have acknowledged all sources, and identified any content taken from elsewhere.

If you have used any code (e.g. open-source code), reference designs, or similar resources that have been produced by anyone else, you must list them in the box below. In the report, you must explain what was used and how it relates to the work you have done.

I have not used any resources produced by anyone else.

You can consult with module teaching staff/demonstrators, but you should not show anyone else your work (this includes uploading your work to publicly-accessible repositories e.g. Github, unless expressly permitted by the module leader), or help them to do theirs. For individual assignments, we expect you to work on your own. For group assignments, we expect that you work only with your allocated group. You must get permission in writing from the module teaching staff before you seek outside assistance, e.g. a proofreading service, and declare it here.

I did all the work myself, or with my allocated group, and have not helped anyone else.

We expect that you have not fabricated, modified or distorted any data, evidence, references, experimental results, or other material used or presented in the report. You must clearly describe your experiments and how the results were obtained, and include all data, source code and/or designs (either in the report, or submitted as a separate file) so that your results could be reproduced.

The material in the report is genuine, and I have included all my data/-code/designs.

We expect that you have not previously submitted any part of this work for another assessment. You must get permission in writing from the module teaching staff before re-using any of your previously submitted work for this assessment.

I have not submitted any part of this work for another assessment.

If your work involved research/studies (including surveys) on human participants, their cells or data, or on animals, you must have been granted ethical approval before the work was carried out, and any experiments must have followed these requirements. You must give details of this in the report, and list the ethical approval reference number(s) in the box below.

My work did involve human participants, ethics approval number 48085.

Contents

| | |
|---|-----------|
| Acknowledgements | xv |
| 1 Introduction | 1 |
| 1.1 Context | 1 |
| 1.2 Requirements | 1 |
| 1.3 Contribution | 2 |
| 2 Background Research | 5 |
| 2.1 Market Analysis | 5 |
| 2.2 Detection Techniques | 7 |
| 2.3 PC Software | 10 |
| 2.4 System Architecture | 10 |
| 3 System Design | 13 |
| 3.1 Line Signal Detection | 13 |
| 3.2 Transponder Transmission | 18 |
| 3.3 Line Signal Generation | 21 |
| 3.4 Exporting Data | 26 |
| 3.5 Power Supply and User Interface | 27 |
| 4 Hardware Implementation | 29 |
| 4.1 Circuit | 29 |
| 4.2 Casing | 34 |
| 4.3 Circuit Board | 36 |
| 4.4 Assembly | 39 |
| 5 Software Implementation | 41 |
| 5.1 Architecture | 41 |
| 5.2 Timing | 44 |
| 5.3 User Interface | 46 |
| 6 Testing and Evaluation | 49 |
| 6.1 Practicality | 49 |
| 6.2 Timing | 52 |
| 6.3 Commercial Viability | 57 |

| | |
|--|-----------|
| 7 Conclusions | 61 |
| A Project Brief | 63 |
| B Example Cycling Venue Risk Assessment | 65 |
| C Bill of Materials | 67 |
| D Test Race Data | 75 |
| E Project Management | 77 |
| F Design Archive | 81 |
| Bibliography | 83 |

List of Abbreviations

| | |
|---------------|---|
| ACK | Acknowledgement |
| ASK | Amplitude Shift Keying |
| BOM | Bill of Materials |
| CAD | Computer Aided Design |
| CRC | Cyclic Redundancy Check |
| DMA | Direct Memory Access |
| EMF | Electromotive Force |
| IC | Integrated Circuit |
| ID | Identification |
| IO | Input Output |
| IP | Ingress Protection |
| ISR | Interrupt Service Routine |
| LDR | Light Dependant Resistor |
| LED | Light Emitting Diode |
| MCU | Microcontroller Unit |
| MOSFET | Metal Oxide Semiconductor Field Effect Transistor |
| MOSI | Master Out Slave In |
| PC | Personal Computer |
| PCB | Printed Circuit Board |
| RAM | Random Access Memory |
| RF | Radio Frequency |
| RFID | Radio Frequency Identification |
| RMS | Root Mean Squared |
| RSSI | Received Signal Strength Indication |
| RX | Receive |
| SD | Secure Digital |
| SMD | Surface Mount Device |
| SOC | System on Chip |
| SPI | Serial Peripheral Interface |

| | |
|----------------------|-------------------------------|
| TCP | Transmission Control Protocol |
| <b b="" twi<=""> | Two Wire Interface |
| <b b="" tx<=""> | Transmit |

List of Figures

| | | |
|------|---|----|
| 2.1 | Diagram showing general electronic timing system overview. | 5 |
| 2.2 | Diagram showing inductive vs radiative transmission. Reproduced from [1]. | 8 |
| 2.3 | Diagram of various decoder/transponder interfaces implemented in existing products. | 8 |
| 2.4 | Image showing circuit board of the Race Result decoder [2]. | 9 |
| 2.5 | Image showing circuit board of the MyLaps decoder [3]. | 9 |
| 2.6 | Diagram showing proposed system overview. | 10 |
| 3.1 | Diagram showing breakdown of system elements. | 13 |
| 3.2 | Simulation results showing field strength vs location relative to start/finish line. | 14 |
| 3.3 | Simulation results showing effect of coil width on field strength at 0.4m above coil. | 15 |
| 3.4 | Test results showing RSSI of AS3930 passing start/finish line. | 15 |
| 3.5 | Test results showing centre detection algorithm iterations. | 16 |
| 3.6 | Simulation results showing time error caused by acceleration. | 17 |
| 3.7 | Simulation results showing distance error caused by acceleration. | 17 |
| 3.8 | Test results showing wake-up time for AS3930. | 18 |
| 3.9 | Graph showing data rate versus power consumption for various wireless technologies. Adapted from [4]. | 19 |
| 3.10 | Test results showing transmission time between two nRF51822 SOCs. | 20 |
| 3.11 | Schematic showing class-E amplifier design. | 21 |
| 3.12 | Simulation results comparing induced EMF in a 4513TC-245XGL Coilcraft coil with the AS3930 sensitivity. | 22 |
| 3.13 | Test results showing an ASK modulated signal demodulated by the AS3930. | 23 |
| 3.14 | Test results showing a Manchester encoded ASK modulated wake-up pattern. | 24 |
| 3.15 | Test results showing class-E amplifier current control using MCP45HVX1. | 25 |
| 3.16 | Test results showing effect of component variation on class-E amplifier performance. | 25 |
| 3.17 | Output log from CrossMgr TCP interface test. | 26 |
| 3.18 | Render of proposed user interface. | 28 |

| | | |
|------|--|----|
| 4.1 | Schematic design for transponder. nRF51822 circuit adapted from Waveshare [5]. | 30 |
| 4.2 | Schematic design for decoder, main board. nRF51822 circuit adapted from Waveshare [5]. | 31 |
| 4.3 | Schematic design for decoder, secondary board. Ethernet circuit adapted from Arduino [6]. | 32 |
| 4.4 | Render of transponder casing, dimensions of 39.4x43x15.4mm. | 34 |
| 4.5 | Wire frame render of transponder casing. | 35 |
| 4.6 | Bocube enclosure range by BOPLA [7]. Selected dimensions of 151x80x90mm | 35 |
| 4.7 | Wire frame render of waterproof button block for decoder. | 36 |
| 4.8 | Version 1.1 of the transponder circuit board layout. | 36 |
| 4.9 | Diagram showing decoder PCB mounting approaches. | 37 |
| 4.10 | Version 1.0 of the decoder circuit board layout. | 38 |
| 4.11 | CAD render of decoder circuit board assembly. | 38 |
| 4.12 | CAD render of decoder assembly. | 39 |
| 4.13 | CAD render of transponder assembly. | 39 |
| 5.1 | Flow chart showing decoder software implementation. | 43 |
| 5.2 | Flow chart showing transponder software implementation and interface with decoder. | 44 |
| 5.3 | Diagram showing layout of system user interface. Generated using [8]. | 47 |
| 5.4 | Diagram showing layout of system menu. Generated using [8]. | 48 |
| 6.1 | Picture of final club cycle race timing system. | 49 |
| 6.2 | Test setup for determining ingress protection rating of decoder. | 51 |
| 6.3 | Test setup for measuring start/finish line detection characteristics. | 53 |
| 6.4 | Test results showing precision of timing system generated using simultaneous transponder detections. | 53 |
| 6.5 | Test results showing precision of timing system generated using single transponder detections. | 54 |
| 6.6 | Histogram of system precision for various test methodologies. | 55 |
| 6.7 | Example outputs from CrossMgr based on test race. | 57 |
| B.1 | Risk assessment for cycling facility often used for club cycling races [9]. | 66 |
| E.1 | Table showing risk analysis. | 78 |
| E.2 | Gantt chart of proposed work. | 79 |
| E.3 | Gantt chart of work completed. | 80 |

List of Tables

| | | |
|-----|---|----|
| 1.1 | Specification of timing system developed in this project. | 3 |
| 2.1 | Specification of existing products. | 6 |
| 3.1 | Table showing errors in calculated centre point of start/finish line. . | 16 |
| 3.2 | Passive RFID frequency properties. Adapted from RFID4U [10]. . . | 19 |
| 3.3 | Simulation results from class-E amplifier component value optimisation. | 22 |
| 3.4 | Component values used in class-E amplifier testing. | 23 |
| 5.1 | Decoder microcontroller resource allocation. | 41 |
| 5.2 | Transponder microcontroller resource allocation. | 42 |
| 5.3 | Detection data transmission protocol. | 45 |
| 6.1 | Estimated costings for club cycle race timing system. | 50 |
| 6.2 | System battery life calculations (Consumption Rate of 0.7)[11][12][13] | 50 |
| 6.3 | Test results showing effect of supply voltage on operating frequency. | 54 |
| 6.4 | Rider transponder allocation for test race. | 56 |
| 6.5 | Test race data for rider JacobD processed by CrossMgr. | 56 |
| 6.6 | Test race results generated by CrossMgr. | 56 |
| C.1 | Estimated BOM for transponder assembly. | 68 |
| C.2 | Estimated BOM for decoder assembly. | 73 |
| D.1 | Test race passing data stored on SD card. | 76 |

Acknowledgements

Thanks to Professor Steve Gunn, project supervisor, for his advice and guidance throughout the project. Further thanks to Professor M.C. Schraefel, second examiner, for her enthusiasm towards the project and suggesting Professor Kirk Martinez to advise on system waterproofing, to whom thanks is also given. Thanks to Luke Anderson at British Cycling for advertising the survey, and thanks to all the clubs that provided responses. Finally thanks to Würth Electronics, Phoenix Mecano, Coilcraft, Keystone Electronics and Samtec for providing product samples.

Chapter 1

Introduction

1.1 Context

As of 2016, British Cycling, the governing body for cycling in Great Britain, reported membership numbers in excess of 125,000, a 60% increase from 2012. With around half of these members taking part in races, 300,000 entrants take part in 4,000 cycling events every year. Many of these races are run by volunteers from one of the 2,200 cycling clubs across the country and therefore minimising the amount of time that must be spent on race organisation, especially results generation, is critical [14]. The Project Brief included in Appendix A discusses the difficulties involved with recording cycling races in more detail.

The aim of this project is to develop an electronic timing system specifically designed for club cycling races, throughout the report this will be referred to as ‘the system’. The system will minimise the amount of time required for volunteer event organisers to produce professional looking and precise results. Improving the efficiency of event organisation will allow cycling clubs to keep up with the continuing increase in participants.

1.2 Requirements

The system must be suitable for use in a club environment, and therefore ease of setup and operation for non-technical users is imperative. Volunteers give up their free time to run cycling races and consequently any additional time required

to learn how to operate the system must be minimised. An intuitive experience is important to enable sporadic users to operate the system successfully.

Setup and operational costs must be minimal to allow clubs to keep race entry costs down, and therefore rider participation up. Clubs might get grants for the initial investment in a system, however, the race fees need to cover the ongoing maintenance. Therefore, rider identification tags must be re-usable.

Ideally, the system will provide highly precise, reliable and accurate results. However, evaluating the importance of each characteristic reveals that while the system must be precise and reliable to ensure confidence in the system from both riders and organisers, the accuracy of the system is less critical. Therefore, when the budget for the system imposes restrictions on these characteristics, accuracy must be compromised over precision or reliability.

With cycle races generally being held outdoors, the system must be weatherproof and consideration must be given to powering the system when mains power is not available. For this reason also, access to a PC must not be assumed and therefore the system should be able to run independently with the ability to transfer data after the race has finished.

Figure B.1 in Appendix B shows the British Cycling risk assessment for a large purpose built cycling facility often used for club racing. The maximum number of riders able to use the facility at any time is one-hundred. This provides a basis for determining the maximum rider capacity required of the system.

1.3 Contribution

The product developed in this project offers a competitive solution to the existing electronic timing system market. Unique features include complete system waterproofing and user replaceable batteries, whilst the performance rivals existing competing products for a fraction of the price and with an emphasis on ease of use. Figure 1.1 summarises the features of the system developed. This report evidences the gap in the market for a low-cost timing solution with suitable performance, and presents the research and development of a system to fill the gap.

| |
|--|
| Capable of recording races with up to 100 riders'. |
| Timing precision of $\pm 0.01\text{s}$ for 90% of detections. |
| Minimum observed reliability of 99.7% for detections. |
| Fully waterproof decoder and transponders. |
| Rechargeable battery for decoder operation without mains power. |
| Decoder battery life of 9 hours. |
| Transponder detection requires single loop of wire across the track. |
| SD card for storing race data and decoder settings. |
| Ethernet port for exporting live race data. |
| Transponders powered by replaceable coin cell battery - CR2032. |
| Transponder battery life of 5 years. |
| Rubber moulding on transponders to protect riders' bikes. |
| Fully compatible with CrossMgr dedicated cycle race timing software. |

TABLE 1.1: Specification of timing system developed in this project.

Chapter 2

Background Research

An electronic timing system is composed of three main components, a PC, a decoder and rider identification devices. Figure 2.1 shows how these components are connected. The decoder is an interface between the rider identification devices, which will be referred to as transponders from now on, and a host PC running software to process the data. In this chapter the implementation of these three system components in existing products will be explored and finally the proposed system architecture will be discussed.

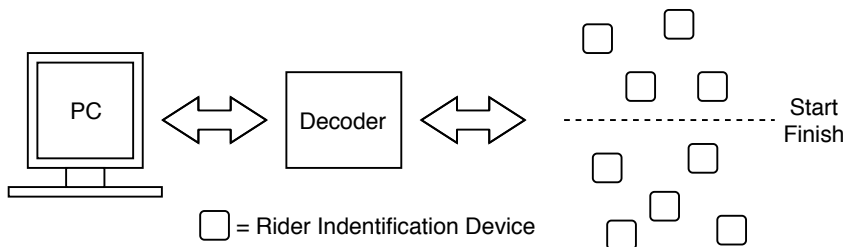


FIGURE 2.1: Diagram showing general electronic timing system overview.

2.1 Market Analysis

Table 2.1 shows existing products that are capable of recording timing data for various applications and their corresponding characteristics. Precision and speed are mainly determined by the detection technique and therefore the hardware of the timing system. The price of the system is influenced by the hardware, but also by the system development time and the business interests of the company.

| Company | System | ID Approach | Precision* | Speed | Decoder Price** | Transponder Price** | |
|--------------------------|---------|-----------------|--------------------|---------|-----------------|---------------------|------|
| RFID RACE TIMING SYSTEMS | Joey | Passive RF | 1mS | N/A | £2,643 | £3.58 | [15] |
| MyLaps | ProChip | Active RF | 3mS (Resolution) | N/A | N/A | £27.89/year | [16] |
| RaceResults | Active | Active RF | 10mS | 150km/h | £1,825 | £50.99 | [17] |
| TAGHeuer | ProTime | N/A | 1mS (Resolution) | 120km/h | N/A | N/A | [18] |
| RCHourglass | DIY | Active RF | N/A | N/A | ~£30*** | ~£5.78*** | [19] |
| MyLaps | RC4 | Active RF | 1.5mS (Resolution) | 120km/h | N/A | £102.48 | [20] |
| MotoSponder | Chute | Passive RF | N/A | 110km/h | £1,206 | £1.51 | [21] |
| Freelap | N/A | Active Magnetic | 20mS (Accuracy) | N/A | £127.40 | £112.33 | [22] |
| LapSnapper | N/A | Active Magnetic | 1mS (Accuracy) | 160km/h | £97.25 | £47.14 | [23] |

* Proper comparison cannot be made between values for precision, resolution, or accuracy. Most companies only provide values for one field.

** A lack of publicly available pricing is assumed to mean the price is high.

*** Since the system cannot be purchased, these are estimates of the BOM.

TABLE 2.1: Specification of existing products.

From Table 2.1 it can be seen that system cost and capability of existing products vary significantly, but not always proportionally. ProChip, Active and ProTime are the dominant systems for the specific application of cycle race timing and all provide precise, high speed solutions at a high cost. Alternative, similarly priced systems such as the RC4, Joey and Chute are designed for different applications and consequently their suitability to cycle races in general varies. The companies FreeLap and LapSnapper both provide significantly lower cost solutions. However, FreeLap is designed for timing single participants and LapSnapper for timing kart races, which requires a significantly lower detection height than cycling races, where the average transponder height is 0.4m. RCHourglass, although not designed for cycle races demonstrates the possibilities for implementing a low cost timing solution.

2.2 Detection Techniques

The majority of existing solutions can be directly compared to RFID or radio frequency identification systems. RFID is used extensively by consumers for payment and travel as well as by industry for access control and asset management. Consequently, there are many variants in the exact implementation of RFID. In the timing implementation discussed in this report the transponder is detected and its time of detection is stored.

The use of active versus passive transponders is the primary difference in the systems listed in Table 2.1. An active transponder carries its own power source, generally a battery, while a passive transponder gets its power from the energy in the interrogation transmission from the reader. Since active transponders include a battery they are capable of longer range transmission than passive alternatives and have capacity for data processing on-board, while passive transponders can be made significantly smaller and produced at less cost than an active alternative. Costs can also be saved with passive devices as they do not contain a radio and are therefore subject to less certification requirements [24]. An advantage of active transponders specific to timing is their speed of activation and response since they do not require energy to be harvested in order to operate. This is reflected in the products shown in Table 2.1.

A further difference in existing systems is the coupling technique used, Figure 2.2 demonstrates the fundamental difference between inductive (a) and radiative (b) coupling. The type of coupling that can be used depends on both the operating

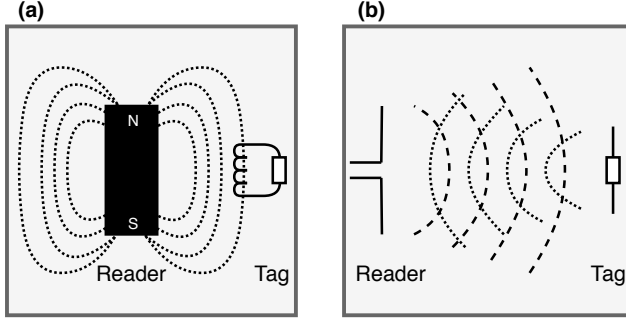


FIGURE 2.2: Diagram showing inductive vs radiative transmission. Reproduced from [1].

frequency and size constraints of both the transponder and decoder. For radiative coupling to be used, the antenna length must be comparable to the transmission wavelength, whereas for inductive coupling, the antenna length can be significantly shorter than the transmission wavelength. Consequently, inductive coupling enables use of lower operating frequencies in compact devices.

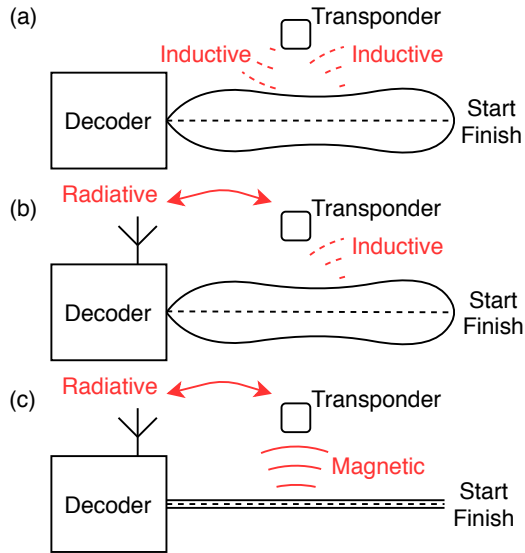


FIGURE 2.3: Diagram of various decoder/transponder interfaces implemented in existing products.

Figure 2.3 shows the different coupling schemes implemented in the existing systems investigated. The major difference between inductive and radiative coupling is their transmission range, while the inductive field decays with distance cubed, the radiative field decays with distance squared [24]. Consequently, configurations (b) and (c) will provide more time for transponders to transmit their presence to the decoder than configuration (a). Configuration (c) uses a permanent magnetic

field to trigger the transponder to report its presence to the decoder, this has the major disadvantage that the transponder cannot verify if the magnetic field is actually from the start/finish line. On the contrary, configurations (a) and (b) can transmit data across the inductive link to verify the signal is that of a start/finish line.

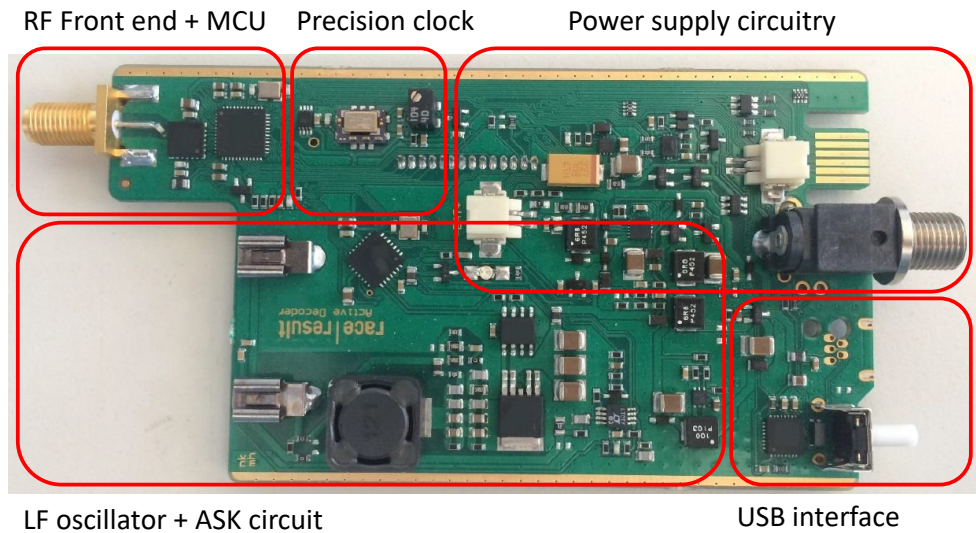


FIGURE 2.4: Image showing circuit board of the Race Result decoder [2].

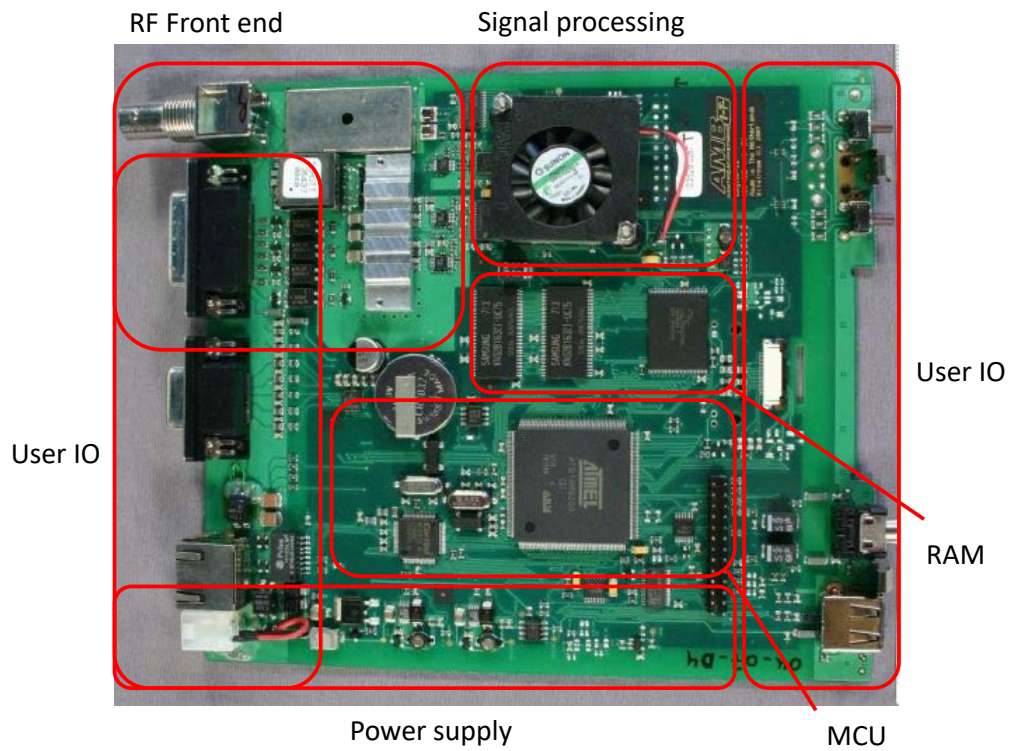


FIGURE 2.5: Image showing circuit board of the MyLaps decoder [3].

Figure 2.4 and 2.5 show internal images from decoders for the Race Results Active and MyLaps ProChip timing systems respectively. Race Results implement configuration (b) from Figure 2.3 while MyLaps implement configuration (a). From the size of the circuit boards and the nature of the components visible in Figures 2.4 and 2.5, it is clear that configuration (b) requires less complex hardware. This is further supported by the corresponding transponder designs [2][3].

2.3 PC Software

CrossMgr is an open source, cycling specific and feature rich timing software that it is ideal for this application. Figure 6.7 in Chapter 6 shows some of CrossMgr's graphical data outputs, while further features include integrated photo finish and live data presentation functionality. Version 2.3.9 is capable of importing Race Result data files as well as communicating via TCP over Ethernet with a Race Result protocol compatible decoder. Race Result provide documentation for the data file format as well as the TCP protocol, enabling integration with CrossMgr software [25].

2.4 System Architecture

Based on this research, a system overview is proposed in Figure 2.6.

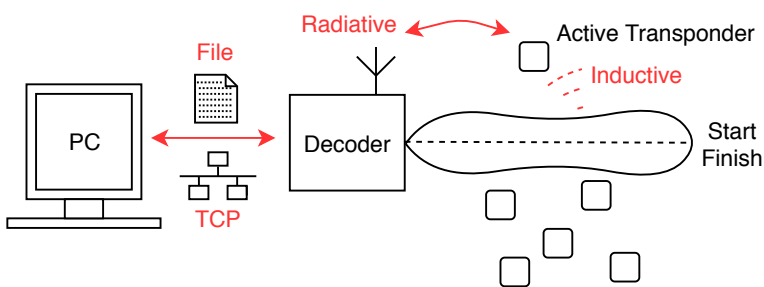


FIGURE 2.6: Diagram showing proposed system overview.

Active transponders are selected over passive transponders due to their better suitability for high speed detection. The size and weight advantages of a passive transponder is negligible since transponders must be mounted to bikes. However, the cost of a passive transponder would be more suited to a club environment than the cost of an active alternative. For this reason, particular emphasis must

be placed on minimising active transponder manufacture and maintenance costs, as well as maximising active transponder lifetime.

An inductive detection approach is taken as it allows transponders to verify the validity of the transmission source, preventing false readings. It also allows the field strength to be varied electronically and the transmission material, a loop of wire, is durable and inexpensive to replace. Furthermore, inductive coupling allows the antenna size to be minimised for low frequency signals, the importance of which are discussed in Chapter 3. This compensates for the larger size of an active transponder versus a passive transponder. From existing product research, it can be seen that this approach provides high precision detection.

Radiative transmission is proposed because of the simplicity of the circuitry required compared to an inductive approach, allowing for minimal BOM and development costs. A further advantage over inductive transmission is the significantly greater range, allowing for successful communication between transponder and decoder further from the start/finish line, therefore, enabling higher speed and higher reliability detection with more participants. The requirement for a longer antenna can be overcome by using high frequency transmission.

A file/TCP interface between the host PC and decoder has the advantage that the protocol is already defined and implemented in CrossMgr. The use of CrossMgr is preferable due to its design for cycling events and large feature base, while remaining easy and intuitive to operate. A TCP connection via Ethernet allows for live results to be displayed, while a file interface enables remote operation and post race result processing as required.

Chapter 3

System Design

The system overview discussed in Chapter 2 can be broken down into the five main sections shown in Figure 3.1. In this chapter, the design of each section is developed and the technical feasibility verified.

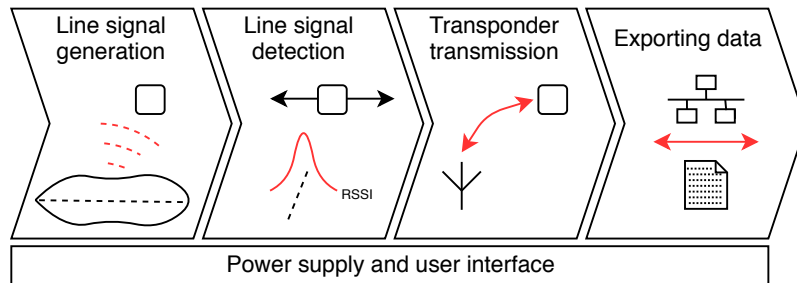


FIGURE 3.1: Diagram showing breakdown of system elements.

3.1 Line Signal Detection

For the system to be able to precisely record rider times, the transponders must be able to detect their position relative to the start/finish line. When considering inductive coupling, the induced EMF in a coil is relative to the rate of change of magnetic flux perpendicular to the coil. If the generating coil is located centrally on the start/finish line, then the EMF induced in the receiving coil will be related to the receiving coil's location relative to the start/finish line. Figure 3.2 demonstrates this concept by plotting the magnetic flux in the Z direction against XY location at a height of 0.4m (the average transponder height when mounted to a bike), relative to a coil with an alternating current flowing through it [26].

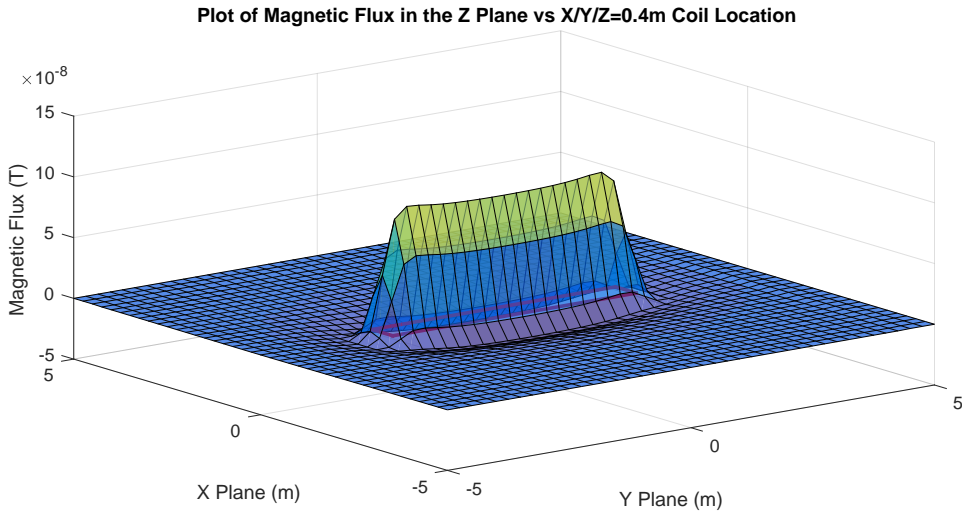


FIGURE 3.2: Simulation results showing field strength vs location relative to start/finish line.

By using a low frequency alternating current for this purpose, for example 125kHz, the introduction of high-permittivity materials, for example a bike, has a minimal effect on the field [24]. Assuming the length of the generating coil is the width of the track, and therefore the width of the generating coil is in the direction of the track, the dimensions of the generating coil can be optimised to maximise magnetic flux at a certain distance, where Optimal Width = Detection Distance $\times \sqrt{2}$ [27]. Figure 3.3 shows the magnetic flux at 0.4m above the generating coil for various coil widths, verifying that $0.4\sqrt{2}$ or 0.56m is the optimal width. This also shows that a generating coil significantly wider than the optimum width produces two peaks, which could produce errors if not accounted for in coil setup or the centre detection algorithm. Figure 3.2 shows that field strength is consistent along the length of the coil, assuming the coil's length is significantly greater than it's width.

Since the lifetime of the transponder must be maximised, low idle power consumption is critical. Kang et al. [28] propose a 125kHz wake-up receiver and compare their results to existing solutions. An ATA5283, MCP2030 and AS3932 are all compared however the ATA5283 has been discontinued and the MCP2030 is only available in larger SMD packages. The AS3932 is a low frequency wake-up receiver with 100uV wake-up sensitivity, programmable wake-up pattern, 1.7uA listening current and provides a digital RSSI value [29]. Bai et al. [30] successfully use the AS3933, a similar IC, to implement a smart shelf active RFID tag.

Combining the AS3930, the single channel version of the AS3932, in the typical application configuration [29] and a 4513TC-245XGL transponder coil from Coilcraft

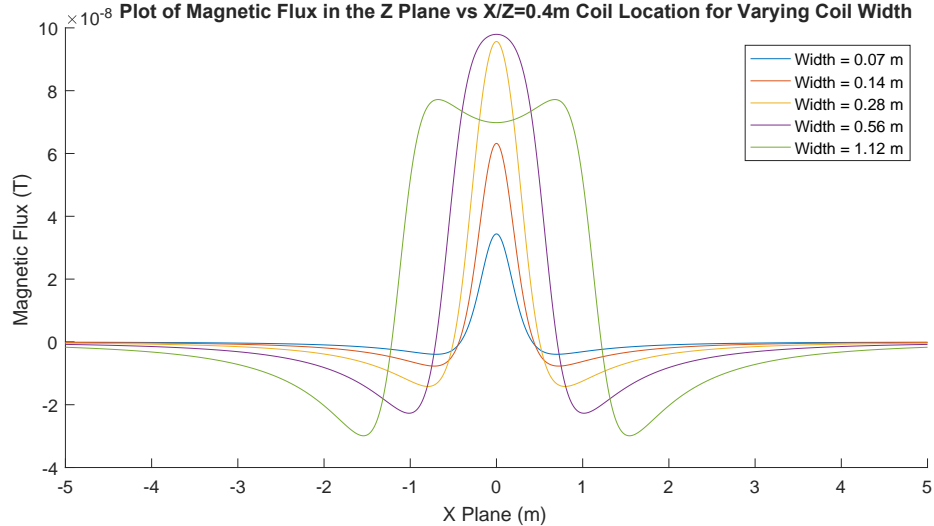


FIGURE 3.3: Simulation results showing effect of coil width on field strength at 0.4m above coil.

with the suggested matching capacitor [31] yields a circuit capable of measuring the RSSI of a 125kHz alternating magnetic field. Figure 3.4 shows the measured RSSI when the detection coil is passed over a generating coil at 32km/h. This is achieved using a stepper motor to spin the detection circuitry and a laser/LDR to determine the actual centre point of the generating coil. Further details of the apparatus used are discussed in Chapter 6. This test demonstrates the potential for precise detection of the generating coil's centre, with roughly one-hundred samples from entering to leaving the field. In this experiment the RSSI never falls to zero since the long wire connections to the AS3930 amplify the 125kHz signal.

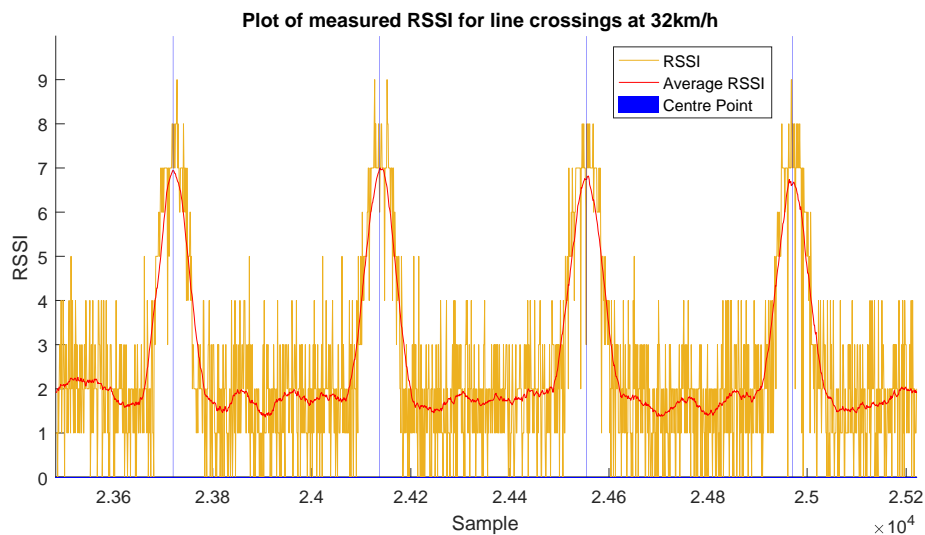


FIGURE 3.4: Test results showing RSSI of AS3930 passing start/finish line.

Figure 3.4 shows the detection technique could provide precise results at a club level cycle race speed. However, for the transponder to identify the centre point of the start/finish line it must be able to determine the peak location of the noisy RSSI signal. Several requirements are placed on an algorithm suitable for this task. Firstly, the amount of computation must be kept to a minimum to enable the host microcontroller to calculate the centre point efficiently. Secondly, the algorithm should calculate the signal peak based on the smallest possible window, to reduce the effects of acceleration on the calculated centre point location. Finally the algorithm does not need to determine the peak location in real time, as the data can be processed once the transponder has fully passed the start/finish line.

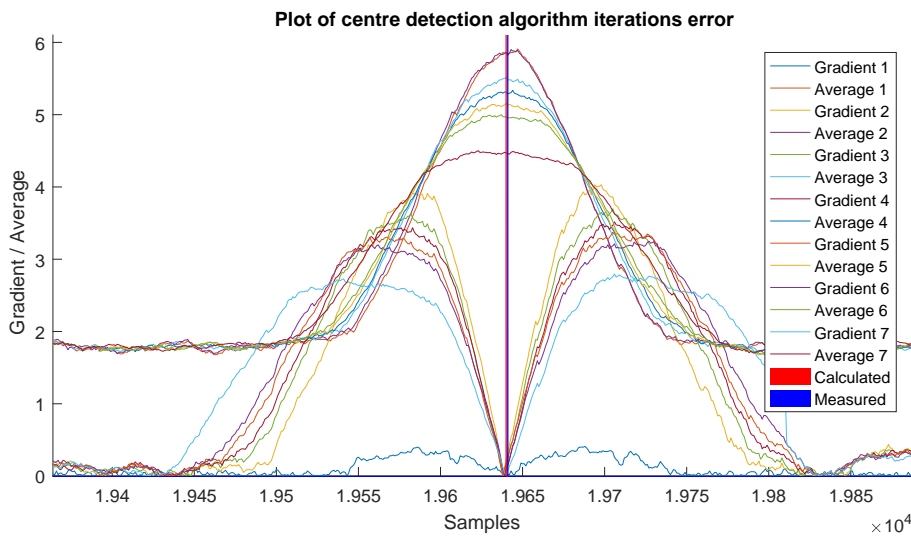


FIGURE 3.5: Test results showing centre detection algorithm iterations.

The output of an algorithm based on the above requirements is shown in Figure 3.5. An iterative approach is taken to calculate successive rolling average and gradient values for each sample, based on a sample window equal to the number of samples between inflection points on the signal curve. For the sample shown in Figure 3.5 this locates the centre point with an error of 3ms, while the error for other calculations is shown in Table 3.1. An average error of 0.16ms, and max error of 4ms, from thirty calculations shows that the algorithm is effective and generates results with precision similar to currently available commercial solutions.

| | Value (ms) |
|-------|--|
| Error | -2,4,-4,2,-1,2,-1,2,1,-1,2,-1,1,0,2,1,-2,2,-1,0,3,-2,1,-3,1,1,0,1,1,-1 |

TABLE 3.1: Table showing errors in calculated centre point of start/finish line.

The points of inflection on the signal curve occur at roughly the same separation as the start/finish line width, therefore for a detection height of 40cm with a start/finish line width of 56cm ($40 \times \sqrt{2}$), the sample window used by the algorithm will be roughly 56cm. Based on this distance the theoretical error caused by acceleration is plotted for time and distance in Figures 3.6 and 3.7 respectively. Wilson [32] suggests that the maximum possible retardation of a cyclist is 0.56g or 5.5m/s^2 , assuming a cyclist will never be able to accelerate as quickly as they can decelerate, the error is insignificant in both time and distance for the majority of realistic speeds/accelerations.

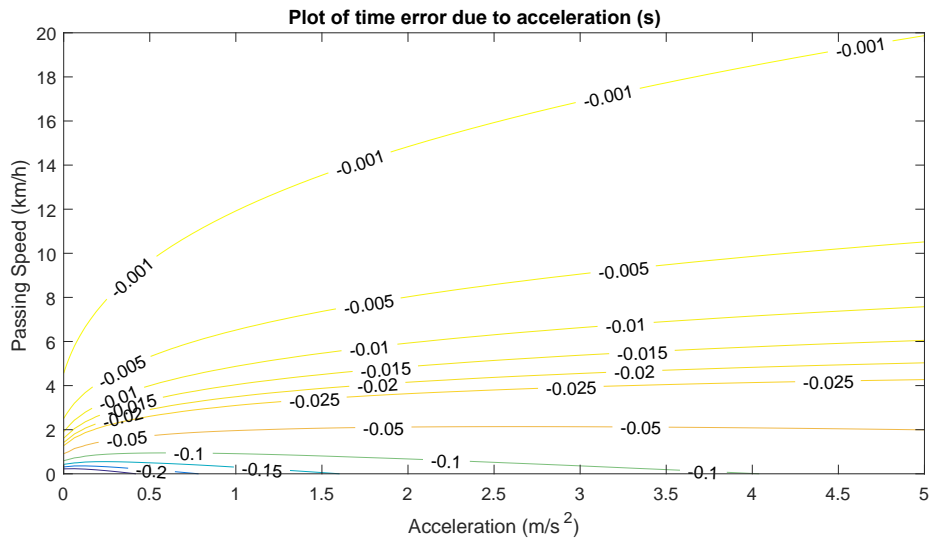


FIGURE 3.6: Simulation results showing time error caused by acceleration.

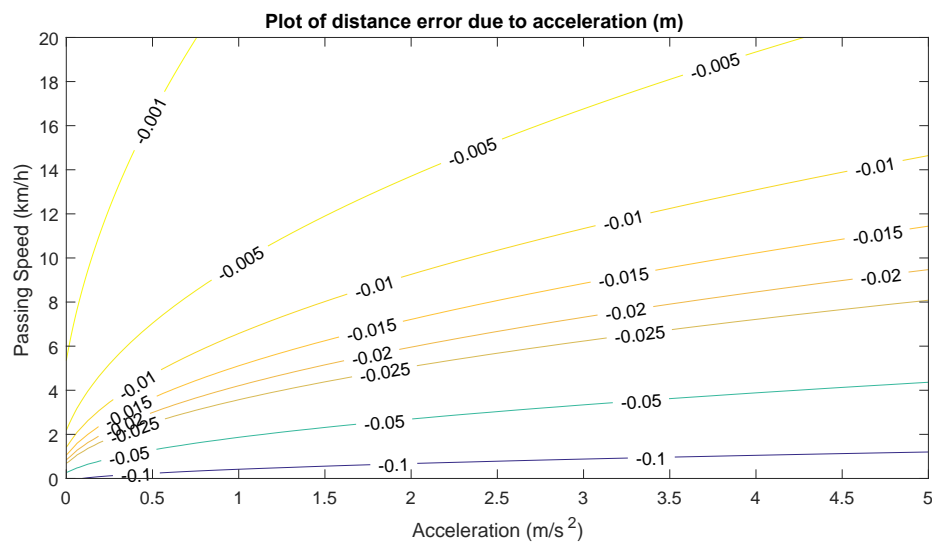


FIGURE 3.7: Simulation results showing distance error caused by acceleration.

Since the purpose of the AS3930 is to wake up the transponder circuit from a low power state, it is important that it is able to do this fast enough for the RSSI pattern shown in Figure 3.4 to be logged. Figure 3.8 shows that with the AS3930 wake-up pattern enabled, the AS3930 takes 136us to assert its wake-up signal, after one complete wake-up pattern is received. This result suggests that the AS3930 has a sufficient response time for the application, while further measurements show that the delay time is of a similar magnitude consistently.

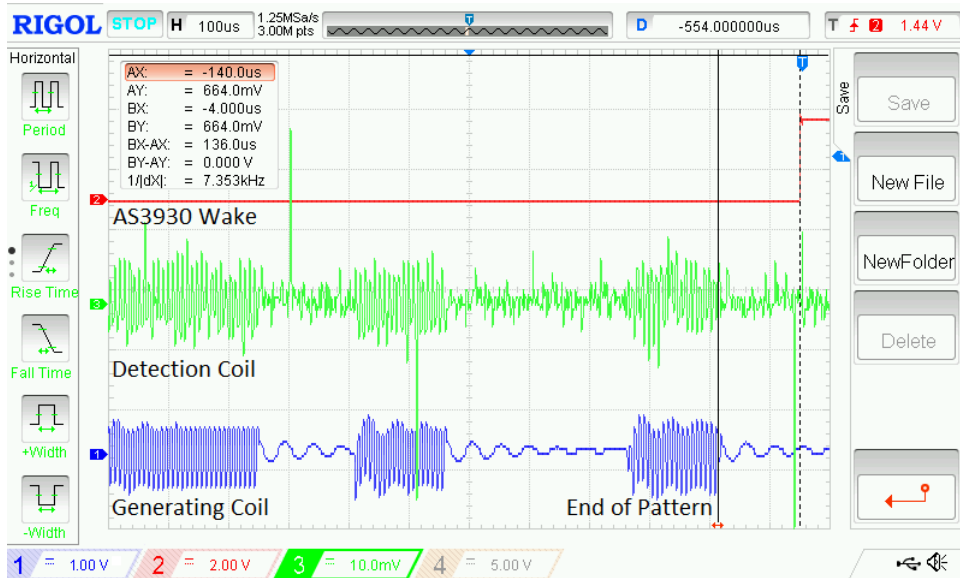


FIGURE 3.8: Test results showing wake-up time for AS3930.

3.2 Transponder Transmission

Once a transponder has detected its position relative to the start/finish line, it must be able to relay this information to the decoder circuit. Since it is possible several riders will cross the start/finish line either in quick succession or simultaneously, it is important that the system is able to handle this. The proposed line detection technique will only be able to detect the centre of the start/finish line after the transponder has passed over it. Therefore the transponder will need to relay the time since it was at this point to the decoder. The time this takes must be minimised in order to maximise overall system precision, however, allowing more time for this transmission to occur will enable higher speed and higher reliability transponder detection.

| Frequency | Coupling | Data | Speed | Range | Usage Example |
|---------------|-----------|--------|--------|------------|----------------|
| 125-134kHz | Inductive | Small | Low | 3-5 feet | Access control |
| 13.56MHz | Inductive | Medium | Medium | 1-3 feet | Smart cards |
| 850-960MHz | Radiative | Medium | High | 1-30 feet | Pallet tagging |
| 2.45 & 5.4GHz | Radiative | High | High | 1-300 feet | Toll roads |

TABLE 3.2: Passive RFID frequency properties. Adapted from RFID4U [10].

Table 3.2 compares the implementation of different frequency bands in passive RFID applications. Although passive RFID is a very different technology to that developed in this project, a comparison can be made since the devices are under the same size and similar power constraints. From Table 3.2 it is apparent a high frequency approach would yield higher range, data and speed communications while using radiative transmission as initially proposed.

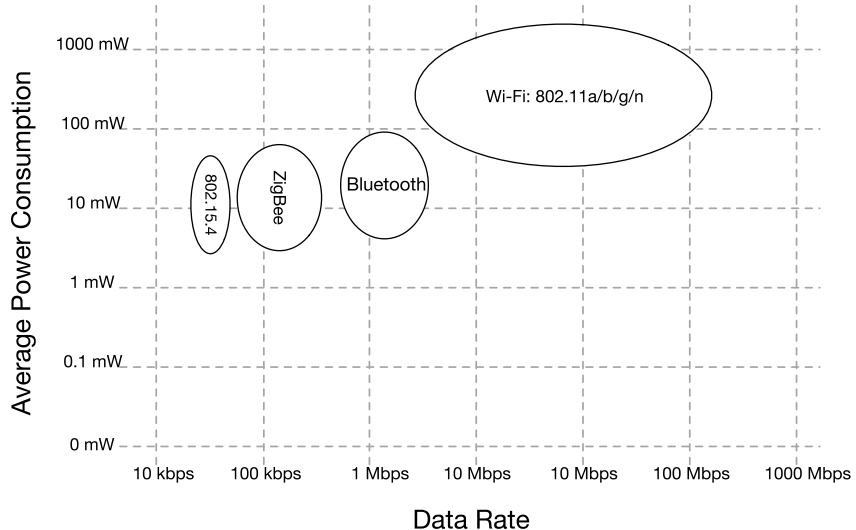


FIGURE 3.9: Graph showing data rate versus power consumption for various wireless technologies. Adapted from [4].

WiFi, Bluetooth, ZigBee and 802.15.4 are all wireless technologies operating in the GHz frequency band. Figure 3.9 compares these technologies in terms of power consumption and data rate, showing that Bluetooth provides an optimal solution, minimising power consumption whilst maximising data rate. However, the Bluetooth protocol is not suited to this application since the maximum number of host connections are limited and a connection must be established before data can be transferred.

Shi et al. [33] and Wangbo [34] successfully use the nRF24L01 by Nordic Semiconductor to implement active RFID tags. The nRF24L01 implements a proprietary

RF protocol with similar data rate and power consumption as Bluetooth, but connection is not required in order to receive data and consequently the number of devices that can transmit to the host is not limited.

An advance on the nRF24L01 is the nRF51822 also by Nordic Semiconductor. The nRF51822 is a SOC featuring a 2.4GHz radio and ARM Cortex M0 in a single package, like the nRF24L01, the nRF51822 implements a proprietary RF protocol with data rates up to 2Mbps and automatic handling of ACK and CRC functionality to ensure reliable communications. The built in ARM Cortex M0 makes the nRF51822 suitable for use as the main microcontroller, as well as the radio transceiver for both transponder and decoder. This reduces the overall system development time and cost by minimising the developer's time spent learning new devices. The use of a SOC also has the advantage of reducing the number of components on the BOM, thus reducing the manufacturing costs. The nRF51822 draws between 0.6uA and 2.6uA in sleep mode and can be woken by a digital pin interrupt [35]. Consequently, combining the nRF51822 with the AS3930 discussed in the previous section would enable a low power, reliable transponder design to be achieved.

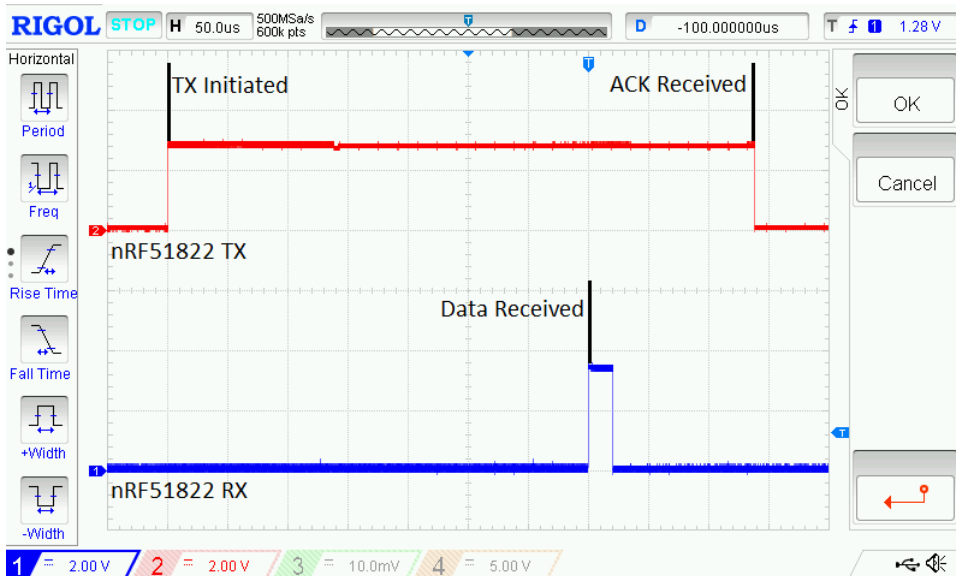


FIGURE 3.10: Test results showing transmission time between two nRF51822 SOCs.

Figure 3.10 shows the results of a transmission time test between two nRF51822 SOCs using the Enhanced ShockBurst protocol to transmit seventeen bytes of data, enough to transmit all of the relevant detection information. From the transmission being initiated to the data being received takes roughly 350us at 2Mbps.

This suggests the use of an nRF51822 SOC would enable reliable communication between the decoder and multiple transponders operating simultaneously.

3.3 Line Signal Generation

To enable the transponders to detect the start/finish line, an alternating magnetic field needs to be generated around the loop of wire centred on the start/finish line as discussed in section 3.1. This magnetic field can be generated by the decoder passing an alternating current through the loop of wire. To enable use of the AS3930 wake-up IC in transponders, the signal must operate between 110kHz and 150kHz, and be capable of modulating a predefined wake-up pattern using an ASK scheme. Since the system may be used in locations where only battery power is available, it is important that the loop power can be regulated across a range of supply voltages.

Lourens [36] suggests the use of a class-D amplifier circuit in either full or half bridge configuration to drive a serial resonant tank as one of the most efficient low frequency drivers. With this configuration a digital square wave signal can be used to generate a sinusoidal current in an output inductance, coupling ASK modulated data to the receiver. An arguably better circuit is that of a class-E amplifier that shares the theoretical efficiency of a class-D amplifier, however, requires only one MOSFET, reducing circuit cost.

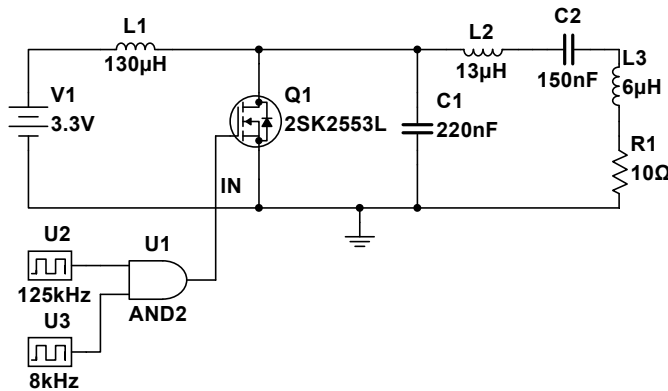


FIGURE 3.11: Schematic showing class-E amplifier design.

Figure 3.11 shows a class-E amplifier design based on an optimised version of the design procedure described by Hagen [37]. The original design procedure takes input arguments Q (quality factor) and R_L (load resistance) to calculate values for

L1, L2, C1 and C2. Through simulations the optimum values for these arguments are determined before the output component values are matched to real world components. Table 3.3 shows the findings of these simulation.

| Value | Quality Factor (Q) | Load Resistance (RL) |
|---------|--------------------------|--|
| High | Reduces response time | Reduces response time & output current |
| Low | Distorts output sinusoid | Produces spice error (0.5 ohm) |
| Optimal | 10 | 1 ohm |

TABLE 3.3: Simulation results from class-E amplifier component value optimisation.

In the circuit in Figure 3.11, L3 represents the impedance of the output coil while R1 is a damping resistor to improve circuit response. U1, U2 and U3 are used to generate a 125kHz, ASK modulated drive signal for the circuit. Simulations show the response time is sufficient to handle the maximum data rate supported by the AS3930 and that the RMS output current produced is roughly 200mA.

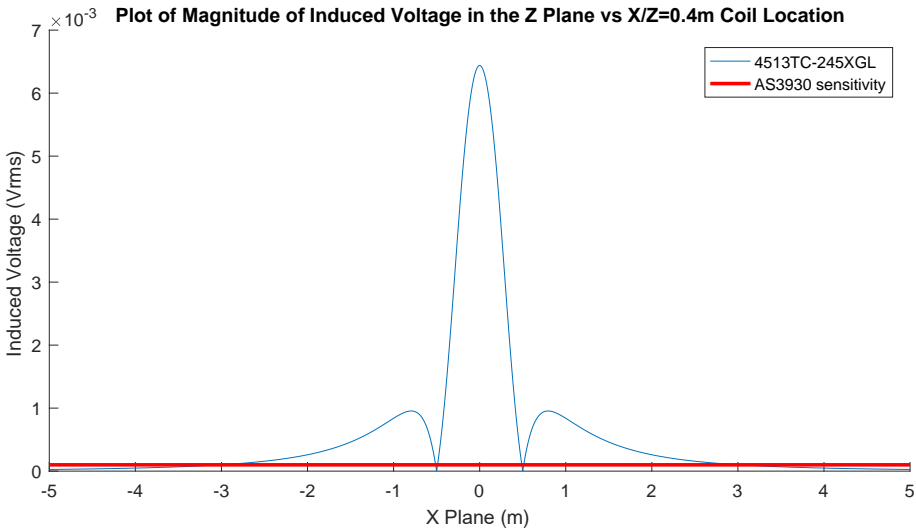


FIGURE 3.12: Simulation results comparing induced EMF in a 4513TC-245XGL Coilcraft coil with the AS3930 sensitivity.

Combining the simulations from section 3.1 and equation 3.1 enables the induced voltage in the 4513TC-245XGL transponder coil to be calculated when the class-E amplifier circuit drives the start/finish loop. Since Coilcraft only proved basic coil characteristics N, S and Q must be estimated: $N \approx 638$, $S \approx 3.585 \times 10^{-6}$, $Q \approx 53$. Figure 3.12 shows the simulated induced EMF in the coil at various locations relative to the start/finish loop versus AS3930 sensitivity. The simulation assumes a start/finish loop of 0.56x5m and a detection height of 0.4m. This shows the

AS3930 would assert wake roughly 3m before crossing the start/finish line, allowing time for the RSSI of the signal to be measured and analysed by the transponder.

$$V_o = 2\pi f_0 N \left(R \sqrt{\frac{C}{L}} \right) S B_0 = 2\pi f_0 N Q S B_0 \quad [27] \quad (3.1)$$

Reproducing the simulation on a breadboard using the components shown in Table 3.4 yields the output shown in Figure 3.13. This shows an 8kHz square wave is successfully transmitted via the inductive coupling between a generating loop and a receiving coil when a class-E amplifier and AS3930 are combined.

| Comp | Value | Comp | Value |
|------|-----------------------|------|-----------------------|
| L1 | RFS1317-124KL (120uH) | L2 | LPS5030-123MRB (12uH) |
| Q1 | 2N7000 | C2 | 150nF polyester film |
| C1 | 220nF polyester film | R1 | 4x 39ohm in parallel |

TABLE 3.4: Component values used in class-E amplifier testing.

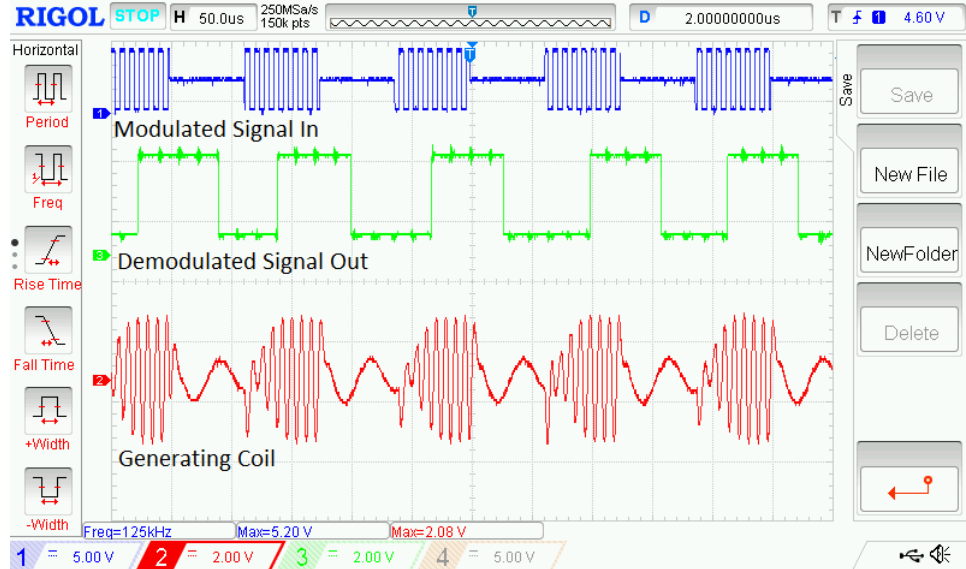


FIGURE 3.13: Test results showing an ASK modulated signal demodulated by the AS3930.

To prevent false wake-up events, the AS3930 is capable of detecting a Manchester encoded, ASK modulated wake-up pattern at a maximum data rate of 8192 bit/s [29]. The ASK modulation can also be used to transmit data, for example the sub-channel that the decoder is operating on. Figure 3.13 shows that the class-E amplifier circuit proposed is capable of modulating a signal at twice this frequency.

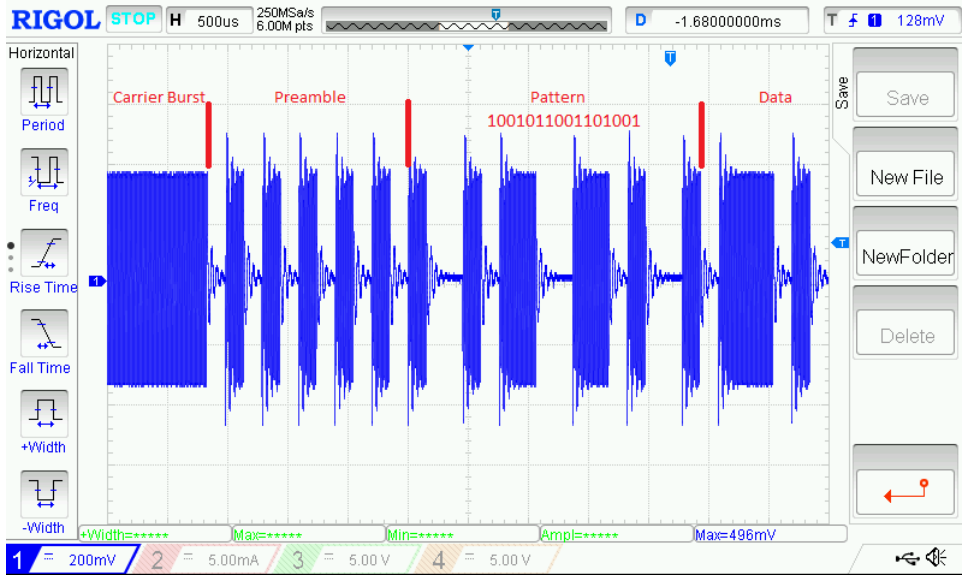


FIGURE 3.14: Test results showing a Manchester encoded ASK modulated wake-up pattern.

To reduce system cost, the Manchester encoded signal should be generated by the same microcontroller running the rest of the decoder functionality. Use of SPI controlled via DMA would enable this signal to be generated without any effect on the other tasks run by the decoder’s microcontroller. Figure 3.14 shows the AS3930’s default wake-up pattern generated by the nRF51822 and transmitted using the class-E amplifier circuit discussed above. A speed of 6552 bit/s is used as it can be matched more precisely to the 250kHz SPI clock.

Since MOSFETs are voltage controlled devices, varying the gate drive voltage can be used to control the output current of the class-E amplifier. A digitally controllable potentiometer such as the MCP45HVX1 can be used solely to achieve this since the MOSFET gate is high impedance [38]. Figure 3.15 shows the gate voltage produced by the MCP45HVX1 and corresponding voltage across R1 from Figure 3.11. Loop current monitoring can be achieved by rectifying and low-pass filtering the voltage across R1. Being able to measure and control output current enables current regulation and detection of an open-circuit start/finish line loop.

To minimise manufacturing costs it is important that manual calibration of the resonant circuit is not required. Figure 3.16 shows how the output signal is affected by variations in true component values within the specified component tolerances. It is assumed capacitors have a 5% tolerance while inductors have a 20% tolerance. From the simulations it is apparent L1 has the biggest effect on the output, with an inductance that is too small the response time is significantly reduced. Therefore,

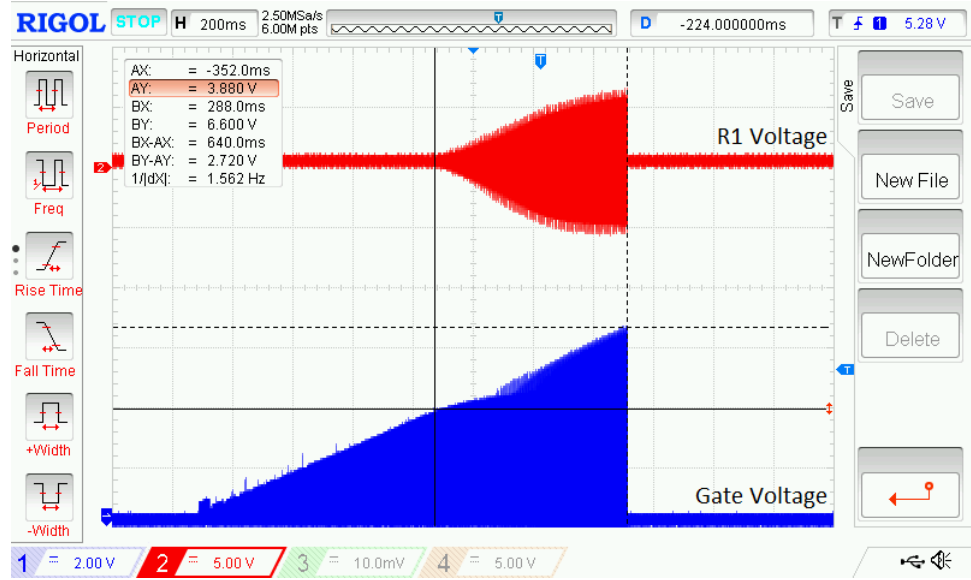


FIGURE 3.15: Test results showing class-E amplifier current control using MCP45HVX1.

it is suggested that L1 be replaced with a 150uH inductor to ensure the circuit response is not affected by component variation.

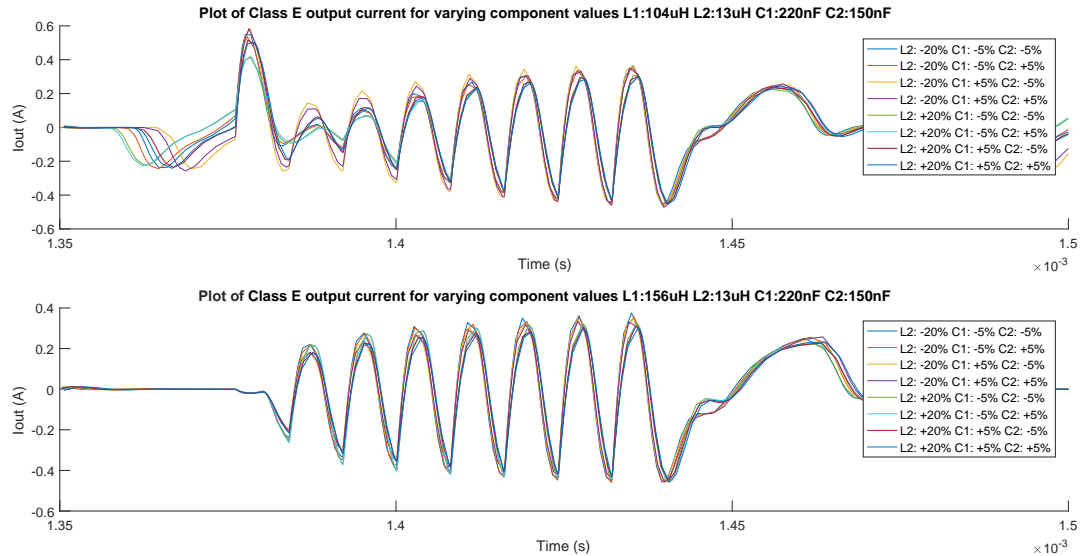


FIGURE 3.16: Test results showing effect of component variation on class-E amplifier performance.

3.4 Exporting Data

Once raw transponder passing data has been collected by the decoder, it must be processed in order to produce race results. Although the computation of race results is simple, data such as rider name versus bib number must be input into the system and consequently exporting raw data to a host PC for processing simplifies this operation.

CrossMgr is able to communicate with decoder devices via TCP to collect the raw data for processing. Figure 3.17 shows how the Race Result TCP protocol is implemented in CrossMgr. In this figure, black text is output from CrossMgr, while red text is output from the TCP server test code. It is clear from this test that data transfer via TCP is possible, and therefore, the use of a W5500 TCP/IP Embedded Ethernet controller for example, would enable communications between the decoder and CrossMgr [39].

```

listening for RFID connection...
connection: <<Attempting to connect to RaceResult reader at 192.168.0.14:3601>>
command: <<sending: GETPROTOCOL>>
6156 192.168.0.14 - GETPROTOCOL - GETPROTOCOL;1.2;1.0;1.2
command: <<sending: SETPROTOCOL;1.2>>
6173 192.168.0.14 - SETPROTOCOL;1.2 - SETPROTOCOL;1.2
status: <<SETPROTOCOL;1.2>>
command: <<sending: GETSTATUS>>
6189 192.168.0.14 - GETSTATUS - GETSTATUS;0000-00-
00:00:02:39 942:1:11111111:1;50;1;49.721,8.254939;1:0;;;;;1:0
status: <<Date: 0000-00-00>>
status: <<Time: 00:02:39.942>>
status: <<HasPower: 1>>
status: <<Antennas: 11111111>>
status: <<IsInTimingMode: 1>>
status: <<FileNumber: 50>>
status: <<GPSHasFix: 1>>
command: <<sending: STOPOPERATION>>
6206 192.168.0.14 - STOPOPERATION - STOPOPERATION;OK
command: <<sending: SETTIME;2018-12-02;12:14:26.933>>
6223 192.168.0.14 - SETTIME;2018-12-02;12:12:50.744 - SETTIME;2018-12-02;12:12:50.744
command: <<sending: STARTOPERATION>>
6240 192.168.0.14 - STARTOPERATION - STARTOPERATION;OK
status: <<STARTOPERATION;OK>>
command: <<sending: GETTIME>>
6257 192.168.0.14 - GETTIME - GETTIME;2018-11-15;12:43:29.942
command: <<sending: 1:1 [0+1=1 passings]>>
6273 192.168.0.14 - PASSINGS - PASSINGS;1
1: tag=QHQNU02, time=2018-12-02 12:14:37.9250, Bib=not found

```

FIGURE 3.17: Output log from CrossMgr TCP interface test.

Alternatively a file written to an SD card by the decoder can be used to import data to CrossMgr, for this reason an SD card socket will also be included in the decoder design.

3.5 Power Supply and User Interface

Since the lifetime of the transponder must be maximised and maintenance costs minimised, a compact rechargeable or replaceable battery is preferable. Non-rechargeable lithium based coin cells with a nominal voltage of 3V are widely available at low cost and would require no additional regulation or charging circuitry. However, this approach would require a waterproof housing with access to the battery, as opposed to a simpler design where the battery is sealed into the case with an external charging port. The latter option would require a rechargeable battery, which in the coin cell form factor is expensive and not produced by many companies. An alternative form factor would be the lithium-polymer battery pack, but these are generally not as compact as coin cells and the additional circuitry required for charging and regulation from the 3.7V nominal voltage would increase initial transponder cost. In sleep mode, the nRF51822 consumes 2.6uA meaning a non-rechargeable coin cell with a capacity of 220mAh [13] would last in excess of five years, making a non-rechargeable coin cell the most cost effective and practical solution.

Based on system requirements, the decoder circuit must also be battery powered and for convenience be rechargeable. With a higher power consumption than the transponder circuit and less stringent size requirements a larger battery can be used. Standard 18650 lithium-ion cells are widely available, low cost and can be connected in series to produce a nominal voltage of 7.4V with a capacity of several Amp-hours. This would provide a suitable voltage for driving the start/finish line signal and could be charged from a 12V supply without requiring significant power dissipation. Since 12V is available in all cars, being able to charge and run off this voltage is essential for a system designed to run in locations where mains power is not available. With current regulation implemented, the start/finish line can be driven at consistent current across the voltage range 5.4V to 12V and can therefore be powered directly from the battery or 12V input. To generate 3.3V from this voltage range, a switching buck regulator should be used to prevent excessive heat generation.

To be suitable for use in a club environment, it is important that the user interface is intuitive to use and system information is presented with clarity. The interface must enable control over recording timing data, present relevant timing and general system information, enable system settings to be changed and prompt the user if the system is not configured correctly while not affecting timing operations. Figure 3.18 shows a proposed user interface design. The display enables lots of information



FIGURE 3.18: Render of proposed user interface.

to be presented in a clear and non-abbreviated fashion. Four push buttons located under the display are dynamically mapped to functions and labelled by the bottom row of the LCD. This minimises the number of buttons required but also ensures the function of each button is clear. An LED and buzzer are used in combination to audibly and visually acknowledge every transponder detection. This provides an intuitive indication as to whether the system is functioning correctly. A second LED indicates battery charging status which enables monitoring of the charge cycle without the decoder being switched on. Finally a physical power switch is used for its intuitive operation, reliability and simplicity.

Chapter 4

Hardware Implementation

The simulation and testing results discussed in Chapter 3 have verified the technical validity of the proposed solution and produced designs for use in the system implementation. In this chapter, the hardware design is finalised and the motivations behind it are discussed.

4.1 Circuit

Figure 4.1 represents the transponder circuit design while Figures 4.2 and 4.3 represent the decoder design resulting from the work in Chapter 3.

The number of components in the transponder circuit is minimised to reduce manufacturing costs. The entire circuit is powered directly from a CR2032 coin cell, the battery voltage of which can be monitored using the direct connection to ADC2. The footprint for a potential divider connected to ADC2 is included for contingency. A parallel RLC circuit tuned to 125kHz enables the AS3930 to provide digital wake-up and de-modulated Manchester encoded signals to the nRF51822 as well as RSSI values via SPI. The nRF51822's built in 2.4GHz radio enables transmission of detection data through the matching network and PCB antenna. JP1 provides connections for firmware programming via the nRf51822's SWD interface as well as serial debugging.

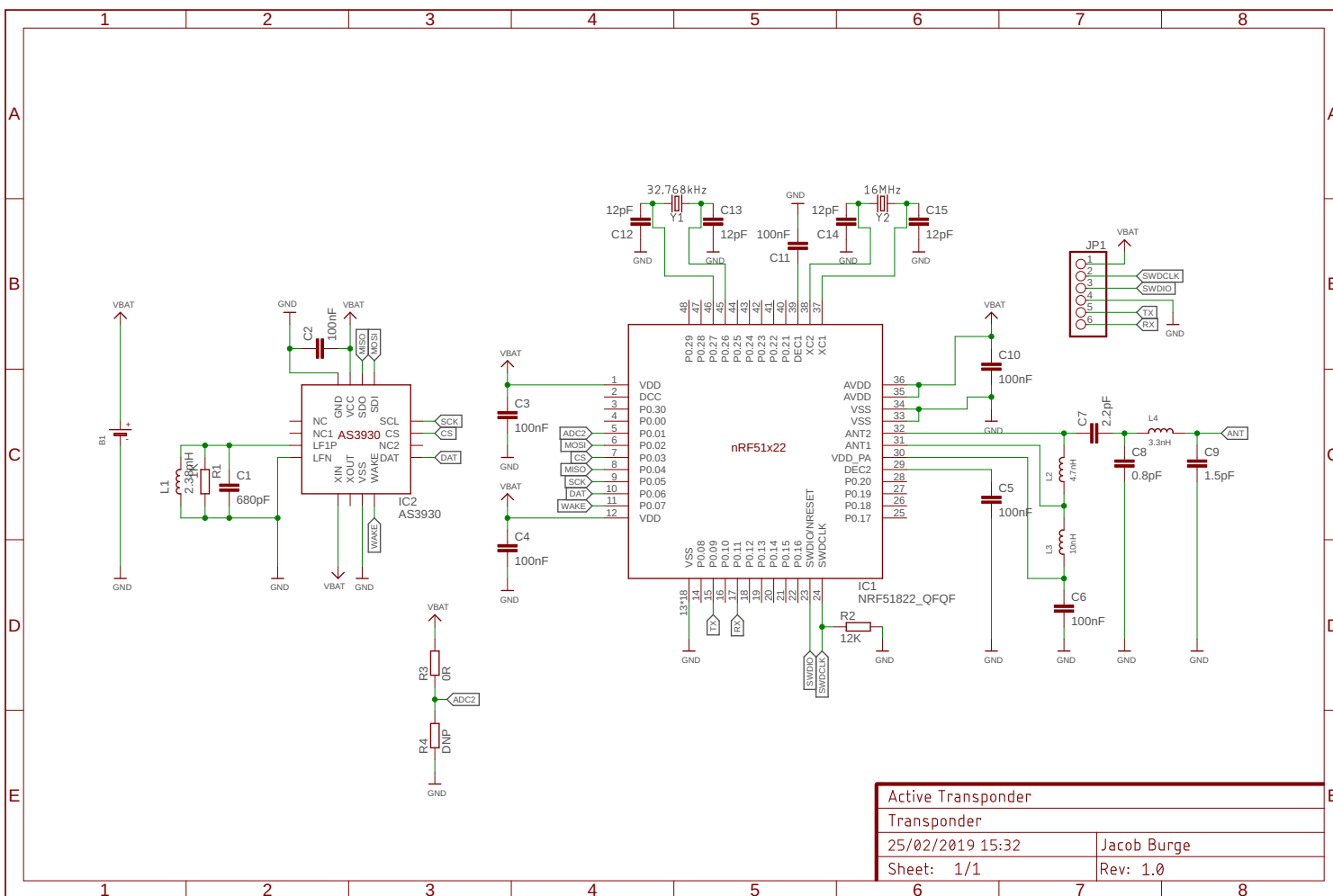


FIGURE 4.1: Schematic design for transponder. nRF51822 circuit adapted from Waveshare [5].

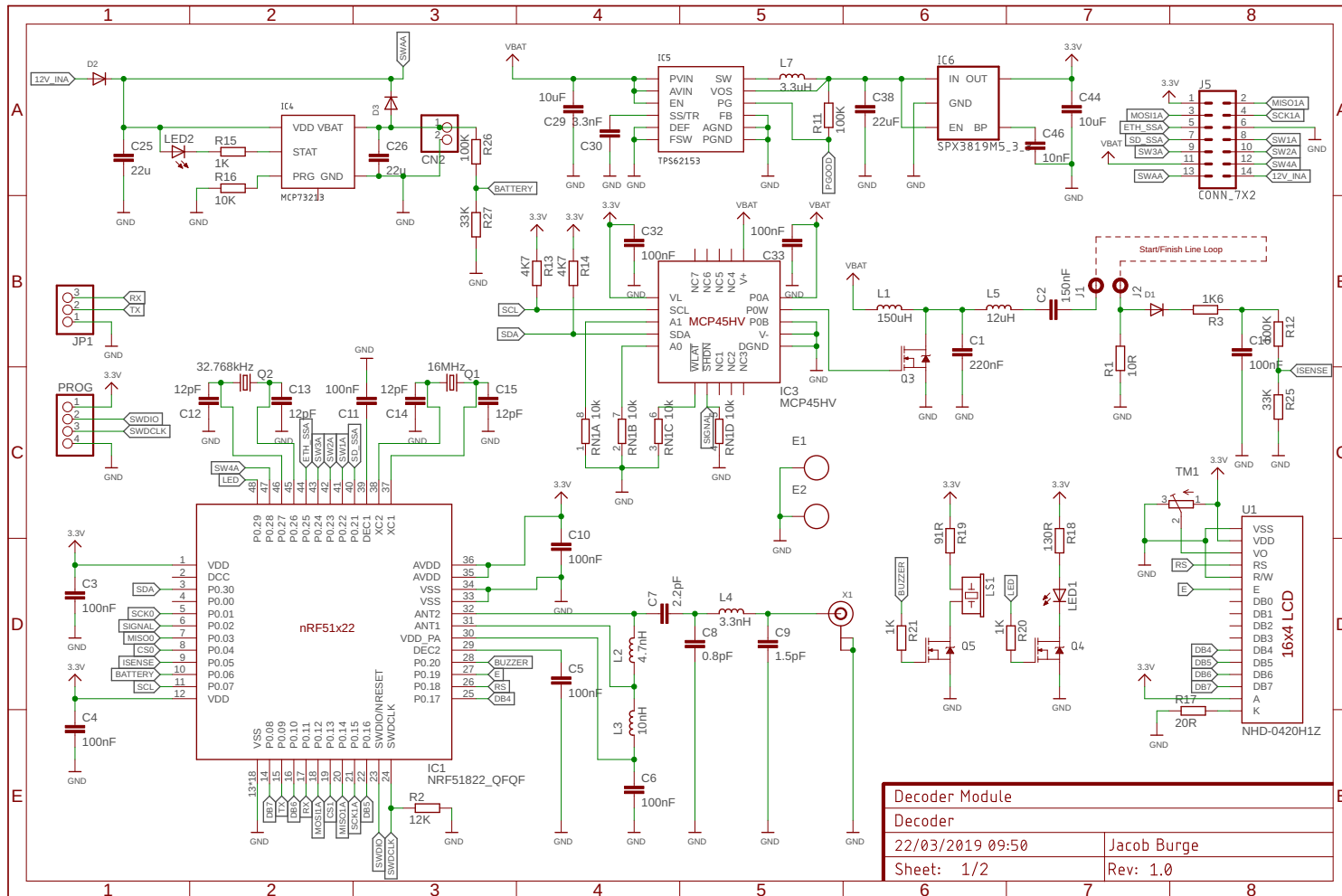


FIGURE 4.2: Schematic design for decoder, main board. nRF51822 circuit adapted from Waveshare [5].

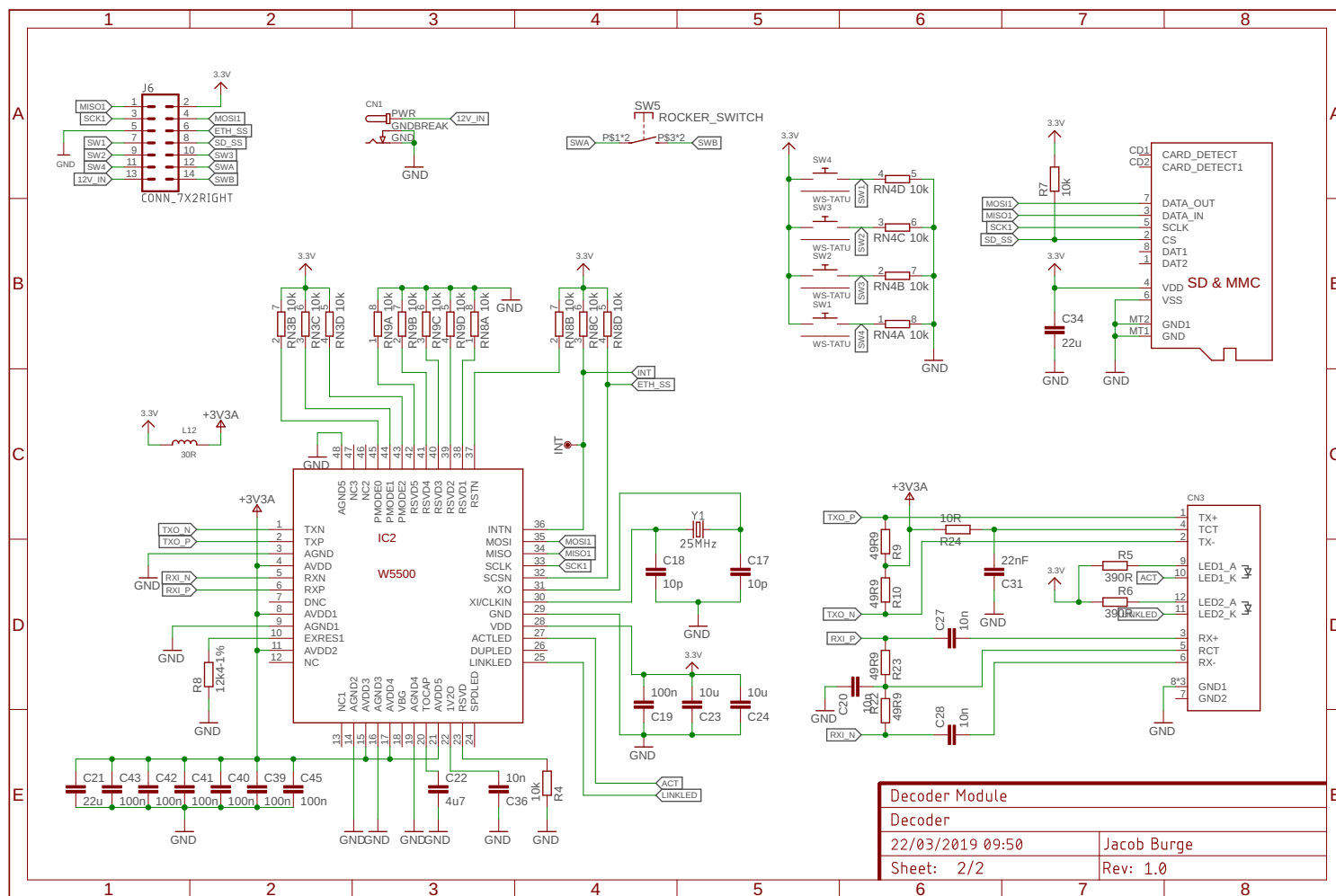


FIGURE 4.3: Schematic design for decoder, secondary board. Ethernet circuit adapted from Arduino [6].

The decoder circuit can be split into three main sections: power supply, detection circuit and user interface. The power supply enables voltage input in the range 5.4V to 12V, either from the battery or DC in connector. The highest voltage source is selected by diodes D2 and D3, if DC in exceeds 9.4V the MCP73213 Li-Ion battery charger IC will charge the battery [40]. LED2 indicates the current charge status while the potential divider formed by R26 and R27 enables the nRF51822 to measure battery voltage on ADC7. The selected voltage source is connected directly to the start/finish line drive circuit and regulated by a TPS62153 buck regulator to 5V, followed by a SPX3819M5 linear regulator to 3.3V, for powering the remaining circuit elements.

The detection circuit is comprised of the 125KHz start/finish line signal generator and 2.4GHz receiver. Waterproof connections to antennas for each are made with banana jack plugs and an SMA bulkhead connector respectively. The decoder circuit includes the same nRF51822 design as the transponders, but an external whip antenna is used to increases the radios range. This increases the manufacturing cost of a single decoder instead of multiple transponders. To generate the start/finish line signal, the regulated Class-E amplifier design developed in Chapter 3 is included. An I2C connection to the MCP45HV enables control of gate drive voltage, while feedback of loop current is provided as a filtered analogue voltage to ADC6. Connection of the MCP45HV's !SHDN pin to an nRF51822 GPIO pin enables the 125kHz carrier and modulated data signal to be applied to the gate of Q3, at the varying voltage set via I2C.

The user interface developed in Chapter 3 is implemented in the following way. The display output is controlled using the reduced 4-bit parallel interface to save nRF51822 GPIO pins, while the display contrast is set using a trimmer pot for calibration during manufacture. Four buttons are connected to pull down resistors, as well as nRF51822 GPIO pins to detect button presses. The passing LED and buzzer are switched by N-channel MOSFETS acting as low side switches to amplify the weak signal from the nRF51822 GPIO pins. To maximise standby battery lifetime and enable charging while switched off, the power switch is located after the battery charging circuit, but prior to any further circuit elements. Finally the Ethernet and SD card interfaces share a single SPI interface with separate chip select signals for device addressing. An Ethernet connector with built in transformers is used to reduce component count and therefore assembly costs. Connectors J6 and J5 provide electrical connection to the secondary PCB, while E1 and E2 provide a mechanical connection. The secondary PCB enables

through hole, right angle, connectors to mount perpendicular to the user interface as discussed in Section 4.3.

4.2 Casing

The requirement for transponders and the decoder to be weatherproof presents unique challenges for both devices. Transponders must be weatherproof while still allowing end users to replace the battery, and the decoder must be weatherproof while still allowing the system to be operated.



FIGURE 4.4: Render of transponder casing, dimensions of 39.4x43x15.4mm.

Existing casing solutions from TAKACHI [41] and OKW [42] enclosures were considered for the transponder housing as they both provide small, waterproof designs, with a battery replacement facility. Both solutions were discounted as neither provide the correct external form factor. Figure 4.4 shows a custom transponder housing design that is compact, waterproof and provides both battery replacement and mounting facilities. The mounting facilities on the custom design include loops for securing the transponder to the fork of a bike, and a rubber moulding to protect the bike paintwork, features which are not present on currently available commercial cases.

Figure 4.5 shows a wire frame render of the custom transponder housing design in Figure 4.4. This shows slots for the transponder PCB to locate in and be

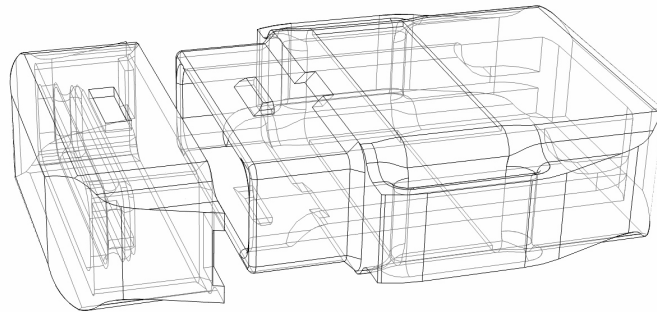


FIGURE 4.5: Wire frame render of transponder casing.

supported by once inside the case. Also visible is a semi-circular channel within the lid to hold an o-ring for sealing the lid to the main body of the housing. Finally a tab and slot in the main body and lid respectively secures the lid, while slots around the main body and lid enable the release of the lid using a common flat-head screwdriver.



FIGURE 4.6: Bocube enclosure range by BOPLA [7]. Selected dimensions of 151x80x90mm

While HAMMOND MANUFACTURING [43] produce several suitable waterproof enclosures for the decoder, the Bocube range from BOPLA [7] shown in Figure 4.6 stands out due to its hinged, quick release and clear lid. This enables non-waterproof elements of the user interface to be fully accessible in dry scenarios, and remain protected, while still visible and partially accessible, in wet scenarios.

Connections for the external whip antenna and start/finish line loop can be implemented with waterproof connectors at a low cost and complexity. Therefore to enable basic operation of the system with the lid closed, at minimum the four buttons should be additionally externally accessible. This enables race data to be recorded to the SD card for processing at a later time, when the scenario allows the lid to be opened. It is assumed users requiring live data via Ethernet will have provisions for keeping technical equipment dry.

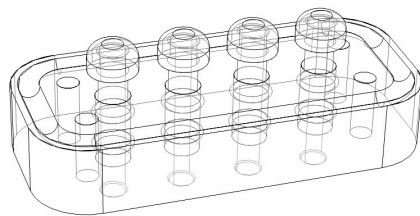


FIGURE 4.7: Wire frame render of waterproof button block for decoder.

Figure 4.7 shows an assembly designed to enable internal buttons to be pressed externally, while maintaining the ingress protection standards of the case. Each actuator is made up of a 4mm aluminium rod passing through two o-rings, secured with a circlip at one end and a plastic cap at the other end. The o-rings are held in place by semi-circular channels in a plastic block which secures to a flat surface with screws, and is sealed to the lid with a gasket around its perimeter.

4.3 Circuit Board

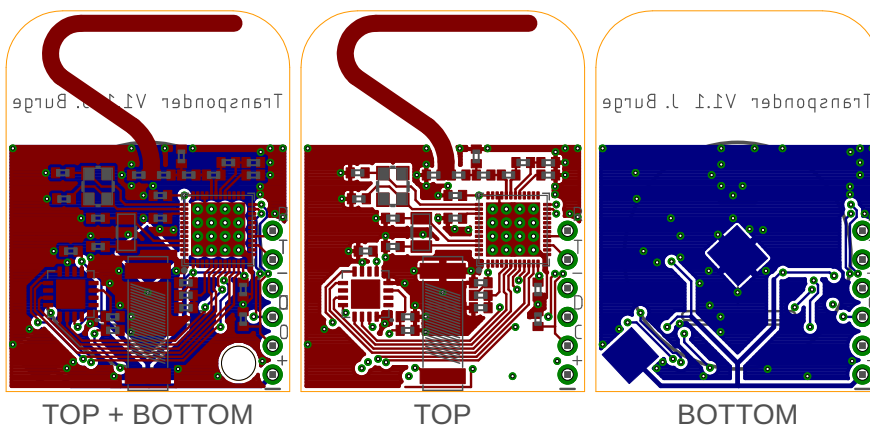


FIGURE 4.8: Version 1.1 of the transponder circuit board layout.

Figure 4.8 shows the second revision of the transponder PCB layout which addresses minor design errors made on the first revision. The main design constraints for the transponder PCB include mounting the 125kHz detection coil centrally, meeting RF design requirements for the 2.4GHz radio, enabling connection of the CR2032 coin cell and ensuring compatibility with the casing design specified in Section 4.2. While placing the 125kHz detection coil centrally does not enable the most efficient PCB layout, it ensures mounting orientation does not effect detection location. To ensure optimum RF performance at 2.4GHz, Kristin [44]’s guidelines are implemented in the design and Nordic Semiconductor [45]’s PCB trace antenna design procedure followed. To prevent the coin cell battery from affecting RF performance, it is positioned away from the antenna. Separate positive and negative terminals are used for the battery connection, while 0402 passives are used throughout the design, all to minimise the amount of space used and ensure compatibility with the custom housing design.

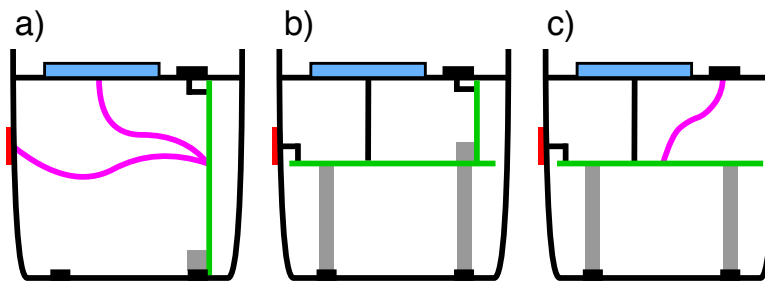


FIGURE 4.9: Diagram showing decoder PCB mounting approaches.

To minimise assembly cost, the decoder PCB shown in Figure 4.10 is intended to mount in the case inline with approach b, shown in Figure 4.9. This has the advantage of requiring no flying wires for connection to externally mounted components, unlike approaches a and c. While the additional components and PCB area required for approach b will increase cost, it is estimated the savings in assembly cost will account for the additional expense.

The main design constraints for the decoder PCB include locating external components correctly, ensuring compatibility with the Bocube range of cases and once again meeting RF design requirements for the 2.4GHz radio. Figure 4.11 shows a CAD render of the PCB assembly including external components and mounting hardware. This shows how the user interface specified in Chapter 3 is achieved, and ensures the final design fits its intended housing. The same 2.4GHz RF design is used as in the transponder design, with the 0402 passives replaced with 0603 passives for consistency with the decoder layout.

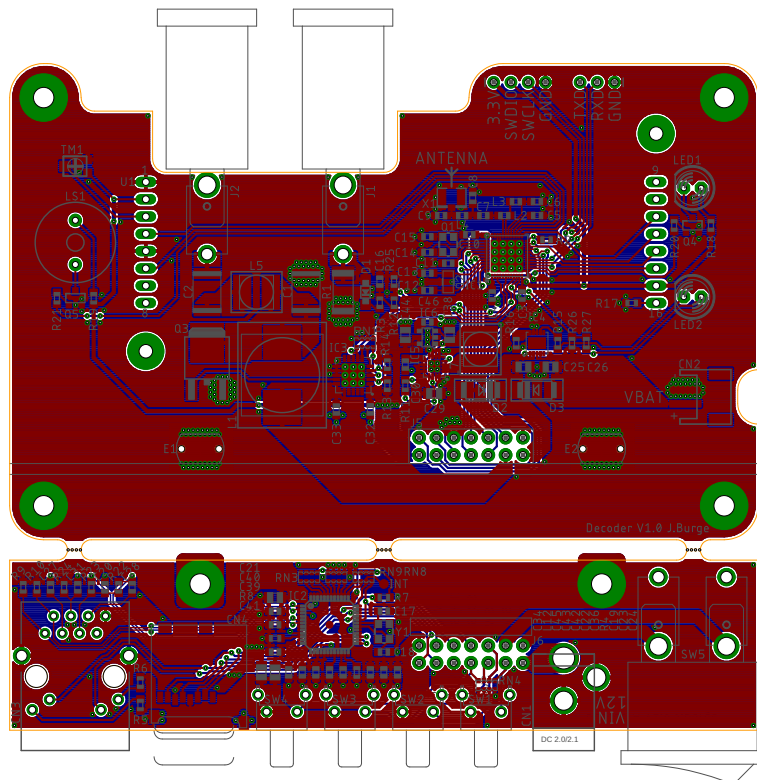


FIGURE 4.10: Version 1.0 of the decoder circuit board layout.

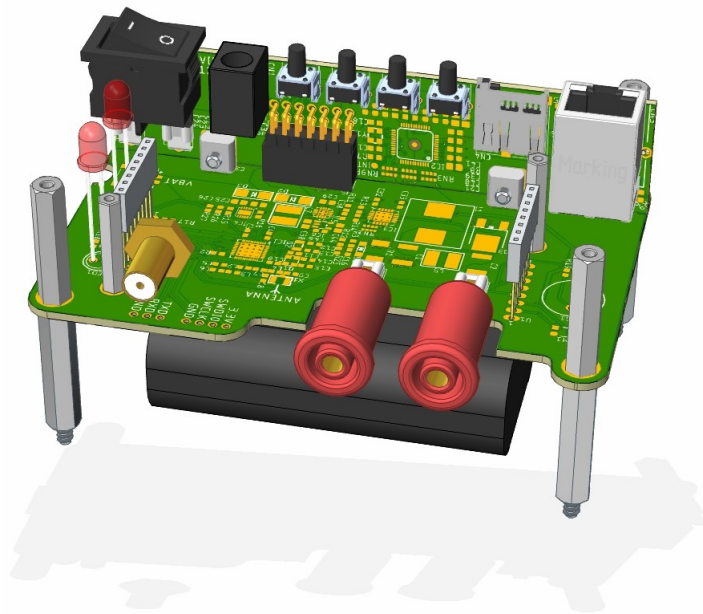


FIGURE 4.11: CAD render of decoder circuit board assembly.

4.4 Assembly

To summarise the work in this chapter, Figure 4.12 and Figure 4.13 show CAD renders of the finalised decoder and transponder hardware assemblies respectively.



FIGURE 4.12: CAD render of decoder assembly.

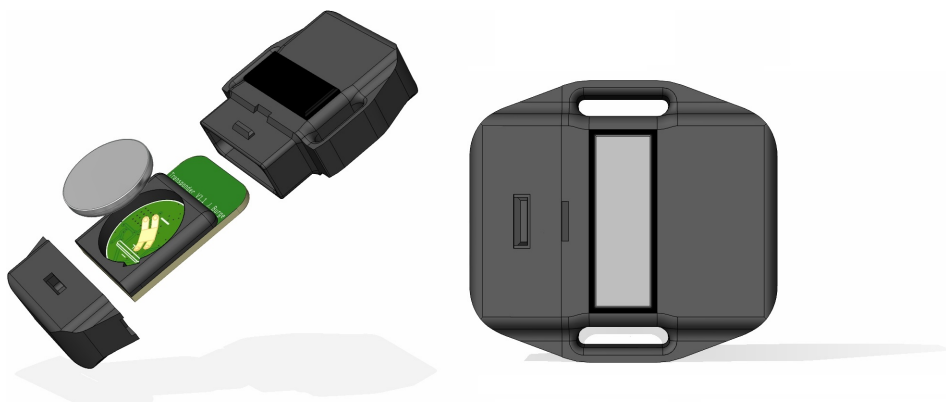


FIGURE 4.13: CAD render of transponder assembly.

Chapter 5

Software Implementation

While Chapter 3 presents individual system modules working independently, for the system to work these tasks must also work in unison. This chapter presents the software architecture developed to achieve this, and discusses the implementation of timing and user interface functionality.

5.1 Architecture

To ensure an efficient software implementation, the hardware resources available on the nRF51822 must be used whenever possible and assigned with task importance in mind. Figure 5.1 shows the finalised resource allocation for the decoder.

| Resource | Allocation |
|----------|---|
| Timer 0 | Microsecond counter/timer. |
| Timer 1 | Start/finish line manchester data modulation. |
| Timer 2 | 125kHz start/finish line signal generation. |
| SPI0 | SD card and ethernet interface. |
| TWI1 | Digital potentiometer gate voltage control. |
| ADC | Battery voltage and start/finish line sense. |
| UART0 | Debug serial interface. |

TABLE 5.1: Decoder microcontroller resource allocation.

Since the device must be able to accurately track time, the only 32-bit timer, Timer 0, is assigned for the purpose. This enables the microseconds since the timer was started to be tracked for up to one hour, when an hour counter is incremented and the timer is reset automatically. The remaining two 16-bit timers are used

to generate the 125kHz start/finish line signal, with Timer 2 providing the carrier frequency and Timer 1 modulating the Manchester encoded data to the channel. The nRF51822's GPIOTE and PPI modules are used in conjunction with Timer 2 to remove the need for an ISR to toggle the output 125,000 times a second. The use of hardware timers and GPIO modules enable these highly frequent tasks to operate with minimal impact on the remaining system tasks.

Although it was initially suggested that DMA could be used to generate the start/finish line signal, it is not possible with the nRF51822 since only two instances of SPI/TWI(I2C) are supported. One instance is required to communicate with the SD card and Ethernet interfaces via SPI, while the other interface is required to set the digital potentiometer value for the start/finish line power control via TWI. However, using timers instead of DMA allows the data bit-rate specified by the AS3930 to be more closely matched.

| Resource | Allocation |
|----------|----------------------------|
| Timer 0 | Microsecond counter/timer. |
| Timer 1 | Manchester data sampling. |
| SPI0 | AS3930 RSSI sense. |
| WDT | Watchdog Timer. |
| ADC | Battery voltage sense. |
| UART0 | Debug serial interface. |

TABLE 5.2: Transponder microcontroller resource allocation.

Figure 5.2 shows the finalised resource allocation for the transponders. Once again Timer 0 is used to track time, where the setup and function calls are identical to the decoder implementation. While Timer 1 is used to sample the Manchester data at a regular interval, the third timer, Timer 2, cannot be used to sample RSSI as SPI function calls cannot be made from an ISR. An important addition to the transponder's list of utilised resources is the watchdog timer. This resets a transponder within one second of it failing to reset the watchdog counter, preventing lock up from draining transponder's batteries and increasing system reliability. This is not implemented on the decoder, as a reset would be equally as damaging to the system's reliability as a lock up.

With resources allocated, the software implementation can be finalised. Figure 5.1 shows how the decoder manages tasks. High priority interrupts are reserved for the time critical tasks of recording transponder detections and modulating start/finish line information. The remaining tasks are called from the main loop after being

triggered by either timer, flag or button press and supported by low priority interrupts for module events. This design ensures a responsive user interface without effecting timing precision or reliability.

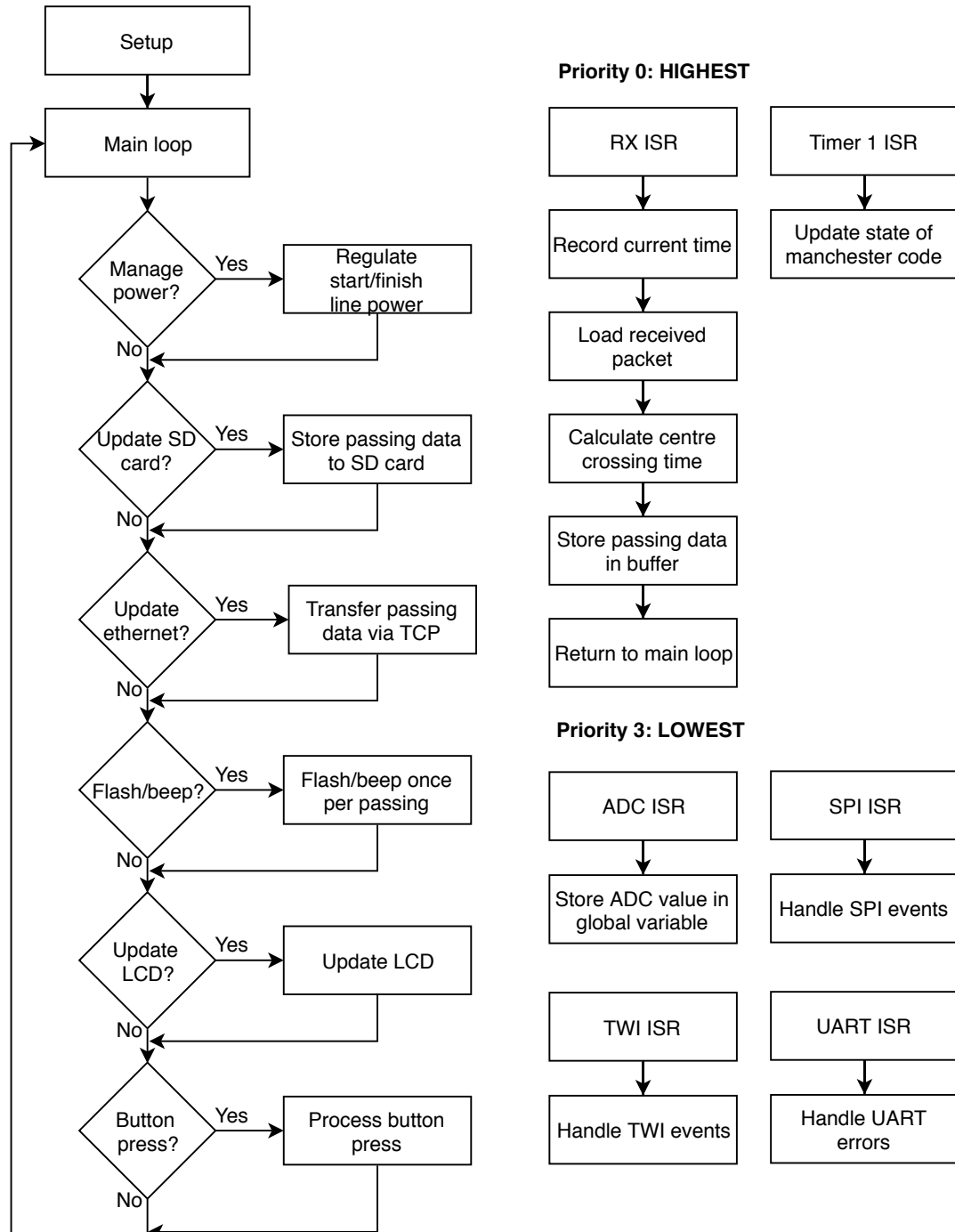


FIGURE 5.1: Flow chart showing decoder software implementation.

5.2 Timing

The work presented in Chapter 3 has shown transponder's centre crossing times can be detected with a precision better than 5ms. To ensure the final system precision is of a similar magnitude, the critical path for recording this time should include as little delay as possible, and ensure a high level of accuracy in data transfer and calculation.

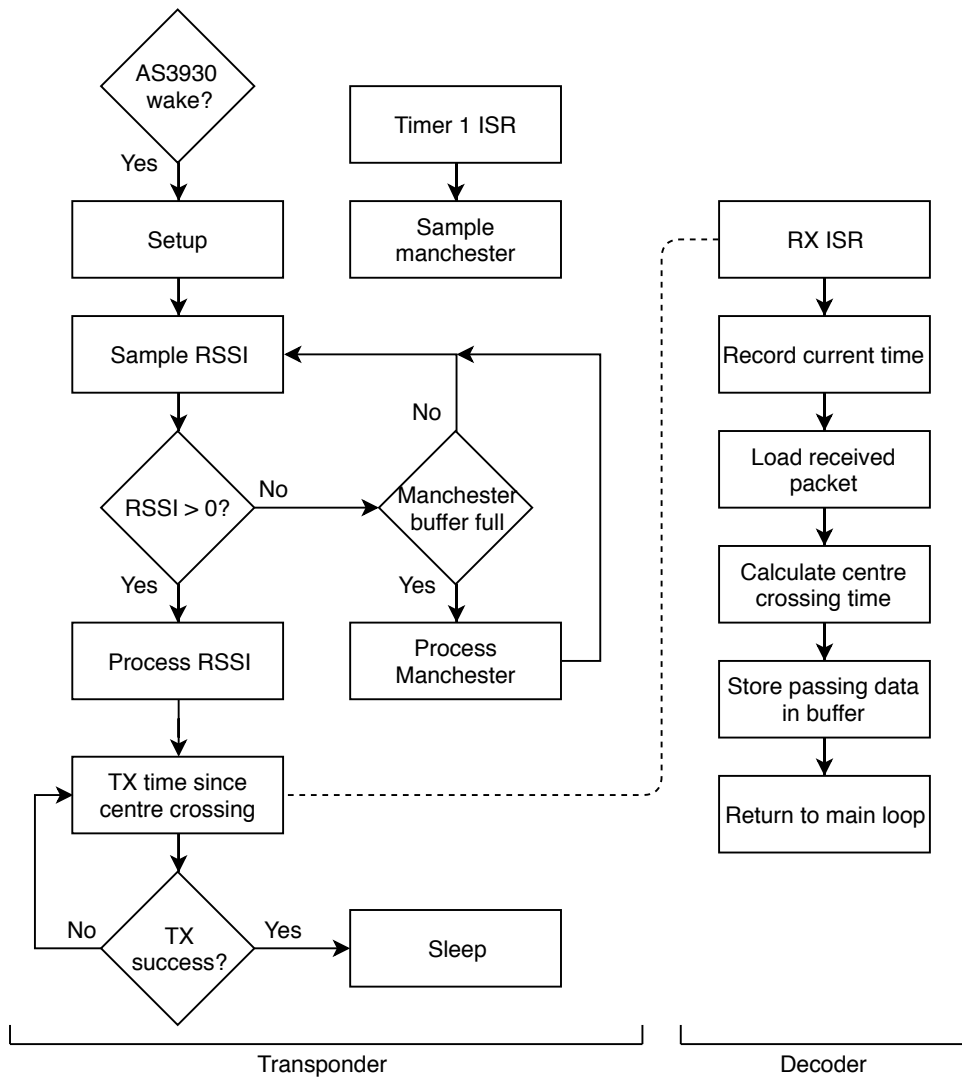


FIGURE 5.2: Flow chart showing transponder software implementation and interface with decoder.

The flow chart in Figure 5.2 shows how the transponder unit manages tasks, and the critical path for recording transponder's centre crossing time. To maximise precision, accuracy and reliability, the following design decisions are made.

Sampling of RSSI begins as soon as transponder setup is complete, this ensures the entire RSSI waveform is captured and prevents significant error in centre detection. Accurately reading the data transmitted by the start/finish line is important as it defines the sub-channel in the 2.4GHz band to be used for transmission of passing data. If this information is not correctly received, all eight sub-channels must be used for transmission, adding delay and therefore potential for inaccuracies. Since the strongest inductive coupling between transponder and start/finish line occurs at the centre point, Manchester data is sampled simultaneously with RSSI data.

Sampling RSSI and Manchester data at high data rates uses a significant amount of the nRF51822's 32kB of RAM. Since RSSI data is 5-bit, it could be split and packed efficiently into bytes. However, this greatly increases run time of the centre detection algorithm and is therefore not suitable. For this reason, the data rate must be balanced between maximising precision and achieving a suitable maximum sample time, sampling at 1kHz achieves this. To minimise the RAM required by the Manchester sampling, but to enable multiple results to be generated, data is processed regularly while RSSI sampling is still taking place. However, processing this data can increase the RSSI sampling interval temporarily, to ensure this is accounted for a time-stamp for each RSSI sample is stored. Due to memory constraints, the time-stamp has to be stored in hundredths of a microsecond.

| Packet Payload, Byte | Allocation |
|----------------------|---------------------------------|
| 0 - 3 | Transponder ID |
| 4 - 7 | Time since centre crossing (uS) |
| 8 | Battery voltage - 1000 (mV) |
| 9 | Detected loop ID |
| 10 | Re-transmit counter |
| 11 - 12 | Number of RSSI samples |
| 13 | Max RSSI value |
| 14 | Temperature |
| 15 - 16 | Wakeup counter |

TABLE 5.3: Detection data transmission protocol.

Once sampling is complete, further telemetry measurements are taken and all data is loaded into the packet format shown in Figure 5.3. Finally, the time-stamp corresponding to the centre sample is used to calculate the time since the sample was taken. This time is loaded into the packet and transmission on the received sub-channel is attempted immediately. If no acknowledgement is received, a random delay is executed before the time since the centre sample is recalculated and the packet sent again. applying a random delay prevents repeated packet

collision, while recalculating time since sample ensures the data transmitted is accurate. If the sub-channel was not successfully received, transmission on each channel is attempted until an acknowledgement is received. Once again, time since the centre sample is re-calculated before each attempt.

Receiving a packet causes the decoder's nRF51822 to enter an ISR with the highest priority, acknowledgement is sent to the transmitting transponder automatically. To minimise delay during transmission, the ISR immediately saves the time that the packet was received. The received data is then processed and the actual time of start/finish line crossing is calculated. To minimise execution time of the ISR, passing data is stored to a rolling buffer in RAM, ready to be written to the SD card or transmitted via TCP at a later time. Returning to the main loop makes the decoder ready to receive the next transponder's detection information.

5.3 User Interface

Figure 5.3 and 5.4 show the user interface displayed on the decoder's liquid crystal display. The layout is designed to minimise the time required to refresh the display, whilst maximising clarity and enabling intuitive operation. Since the nRF51822 has no non-volatile memory, system settings are stored on the SD card as a text file. This is advantageous for a system designed for multiple users as personalised settings can be applied automatically.

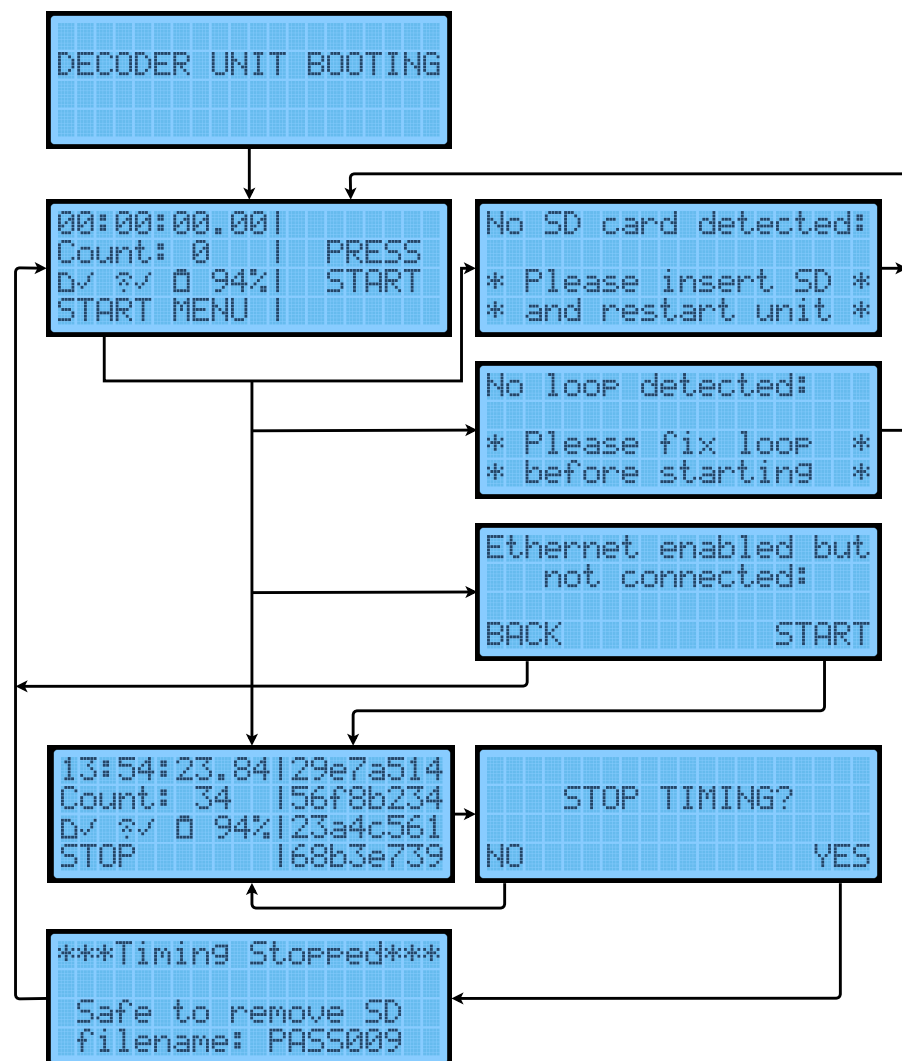


FIGURE 5.3: Diagram showing layout of system user interface. Generated using [8].

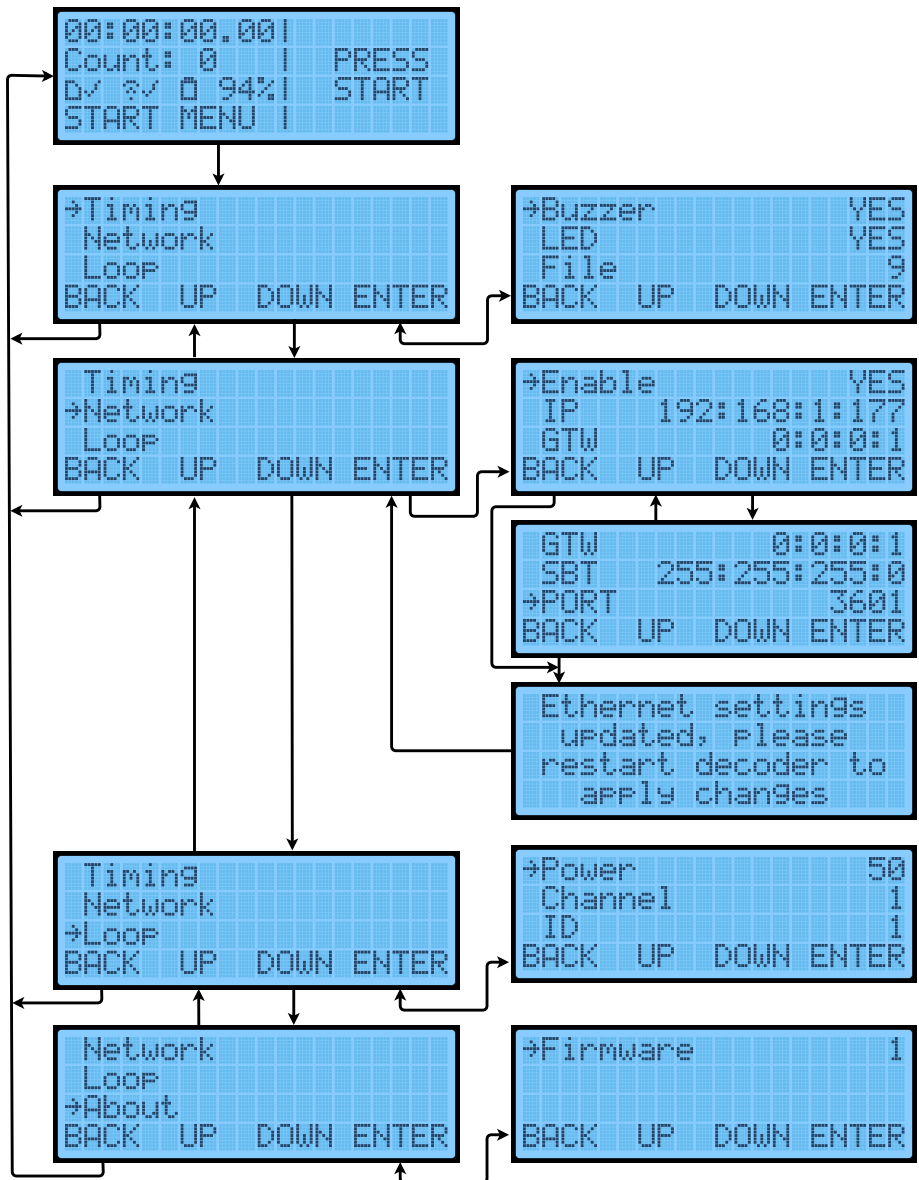


FIGURE 5.4: Diagram showing layout of system menu. Generated using [8].

Chapter 6

Testing and Evaluation



FIGURE 6.1: Picture of final club cycle race timing system.

Figure 6.1 shows the finished club cycle race timing system discussed throughout this report. In this chapter, the system is tested and evaluated for functionality and commercial viability.

6.1 Practicality

Table 6.1 presents system costings based on the bill of materials shown in Appendix C, estimates of overhead costs and target retail prices.

| Manufacture Cost (inc VAT) | |
|-----------------------------------|------------|
| Decoder | £128.63 |
| Transponder | £8.75 |
| Overhead Cost | |
| Premises 2 months | £1,000.00 |
| Development costs 300 Hours | £10,000.00 |
| Plastic tooling | £10,000.00 |
| PCB tooling | £1,000.00 |
| Compliance testing | £10,000.00 |
| Total | £32,000.00 |
| Retail Price | |
| Decoder | £500.00 |
| Transponder | £20.00 |
| Decoder + 100 transponder set | £2,500.00 |
| Profit | |
| Break Even | 22 sets |
| Profit (100 sets) | £117,637 |

TABLE 6.1: Estimated costings for club cycle race timing system.

Table 6.1 shows the system is very competitively priced, when compared to its active timing system counterparts presented in Chapter 2. With minimal development and manufacture costs, a break-even point of twenty-two sets of one decoder and one-hundred transponders can be achieved. Additional profit would be sufficient for sustaining long term customer support and business in general.

| Device | State | Current Consumption | Battery Capacity | Battery Life |
|-------------|----------------|---------------------|------------------|--------------|
| Decoder | Loop 25% 5.4V | 147mA | 2.6Ah | 12.4 hours |
| Decoder | Loop 50% 5.4V | 174mA | 2.6Ah | 10.5 hours |
| Decoder | Loop 75% 5.4V | 220mA | 2.6Ah | 8.3 hours |
| Decoder | Loop 25% 8.4V | 118mA | 2.6Ah | 15.4 hours |
| Decoder | Loop 50% 8.4V | 148mA | 2.6Ah | 12.3 hours |
| Decoder | Loop 75% 8.4V | 185mA | 2.6Ah | 9.8 hours |
| Transponder | Detection 2.7V | 4.50mA | 220mAh | 34.2 hours |
| Transponder | Sleep 2.7V | 2.5uA | 220mAh | 7.0 years |
| Transponder | Detection 3.3V | 4.45mA | 220mAh | 34.6 hours |
| Transponder | Sleep 3.3V | 2.6uA | 220mAh | 6.8 years |

TABLE 6.2: System battery life calculations (Consumption Rate of 0.7)[11][12][13]

While initial transponder cost is significantly less than existing solutions, transponders are also designed to last significantly longer than those solutions. Current market offerings require new transponders to be purchased when battery voltage becomes low. With the system developed in this project, the transponder battery can be replaced at a fraction of both the financial and environmental cost of these systems. Table 6.2 shows battery life calculations based on battery capacity and current consumption for both transponders and the decoder. While transponder battery life is dependant on the time spent in detection versus sleep, it is estimated a CR2032 should last five years under club use. It is assumed average club use involves sixty, twenty lap races per year, with the transponder spending 5s in detection each lap. Decoder battery life is more predictable due to the constant current consumption, even at maximum current consumption, it is sufficient to provide results for an entire day of racing.

The system must be capable of recording races with up to one-hundred riders, although physically testing this is cost prohibitive, it is possible to justify why it should work. Simultaneously passing four transponders over the start/finish has reveals no problems with 2.4GHz interference, and while one-hundred riders could be in the race, the possibility of more than four riders crossing the line simultaneously is low. The second potential problem with many riders crossing the start/finish line in quick succession is recording the data to the SD card, or transferring it via TCP. However, the rolling buffer implemented in RAM has space for 100 entries, meaning enough data could be stored temporarily to account for every rider crossing the start/finish line simultaneously.

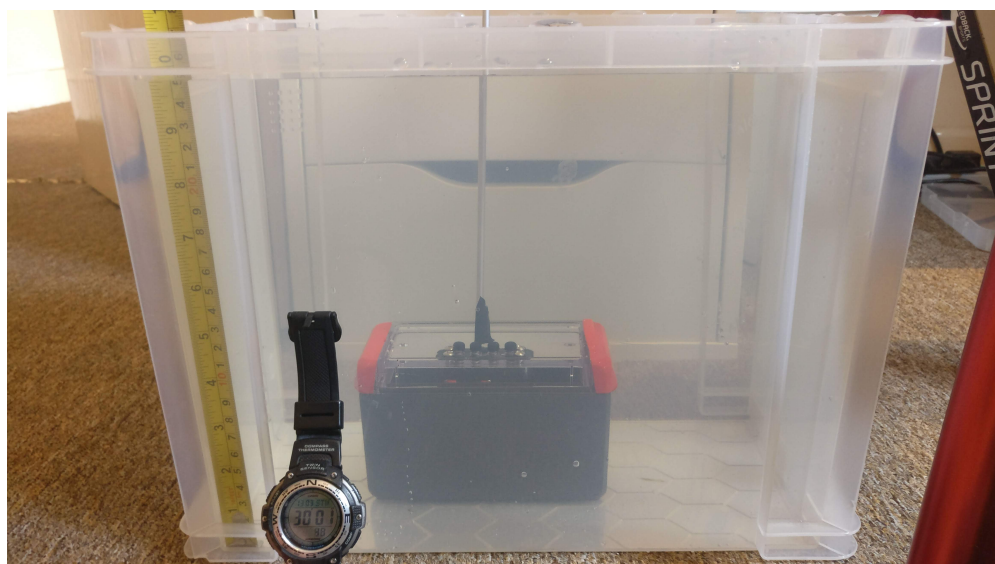


FIGURE 6.2: Test setup for determining ingress protection rating of decoder.

Figure 6.2 shows the setup for testing the decoder's ingress protection rating. Being able to withstand submersion between 15cm and 1m for 30 minutes qualifies the unit for an IP67 rating [46]. Similar testing is used to further qualify the transponder housing as IP67 also. It should be noted that whilst the transponder lid and decoder button block are intended to be sealed with o-rings, 3D prints do not provide a smooth enough surface to form a good seal. For this reason, Instant Gasket silicone sealant by Granville was used for the tests. Further work is required to develop a production ready solution.

Listed below are the five steps to recording a basic race, this shows how simple the system is to operate. Assuming an experienced user has already configured the decoder for the race scenario, all decoder settings will be loaded from the setting file stored on the SD card. A novice user is left with few tasks to setup and record a race. Failure to correctly setup the decoder will prevent recording from starting, and issue the user with a warning and diagnostics message. Since the focus of this project is in the timing hardware, the ease of use of CrossMgr is not evaluated.

1. Setup start/finish line loop and connect it to the decoder.
2. Ensure SD card is inserted in the decoder's SD card slot.
3. Switch decoder on and verify detection by passing a transponder over the start/finish line.
4. Press start to start, then stop and confirm stop to stop.
5. Remove SD card, open CrossMgr and load passing file from SD card.

6.2 Timing

The test setup shown in Figure 6.3 is used to test system precision and reliability. Precision data for the centre detection algorithm presented in Chapter 3 verifies that with a loop power of 50 set on the decoder, and despite the generating coil being of a similar width and length, the magnetic field around the coil is as expected. If more space were available for testing, line length could be increased to satisfy the recommendations made in Chapter 3, however, this is not expected to significantly effect the results. The apparatus shown in Figure 6.3 enables devices under test to be rotated at speeds up to 27km/h, while the speed, LDR value and any device information are reported to a PC via a serial connection. Aiming a low

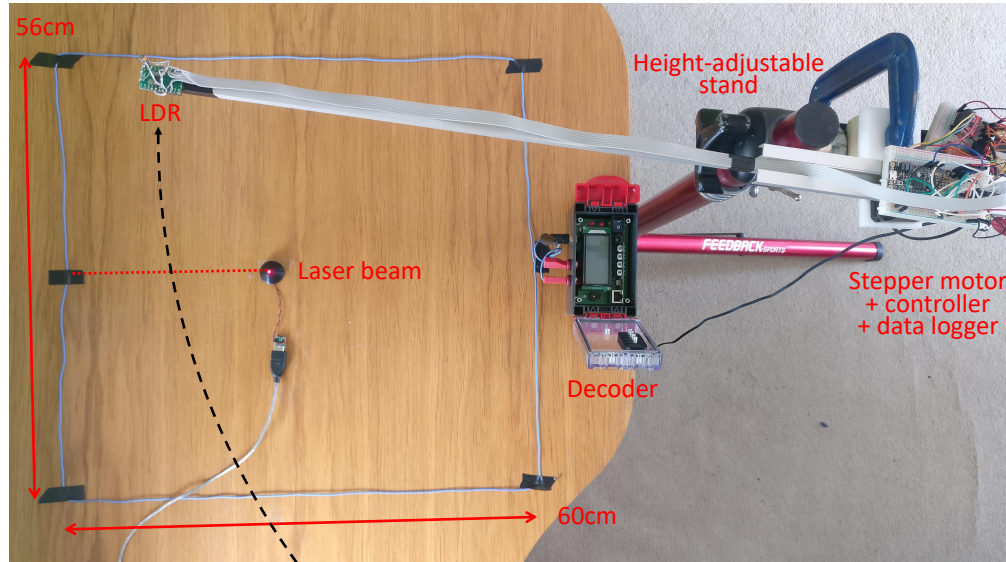


FIGURE 6.3: Test setup for measuring start/finish line detection characteristics.

power laser at the LDR while the armature is directly above the centre of the line provides a reference to this location in the logged data. The maximum speed is limited by the maximum angular velocity of the stepper motor, although 27km/h is considered a representative speed of club cycle races.

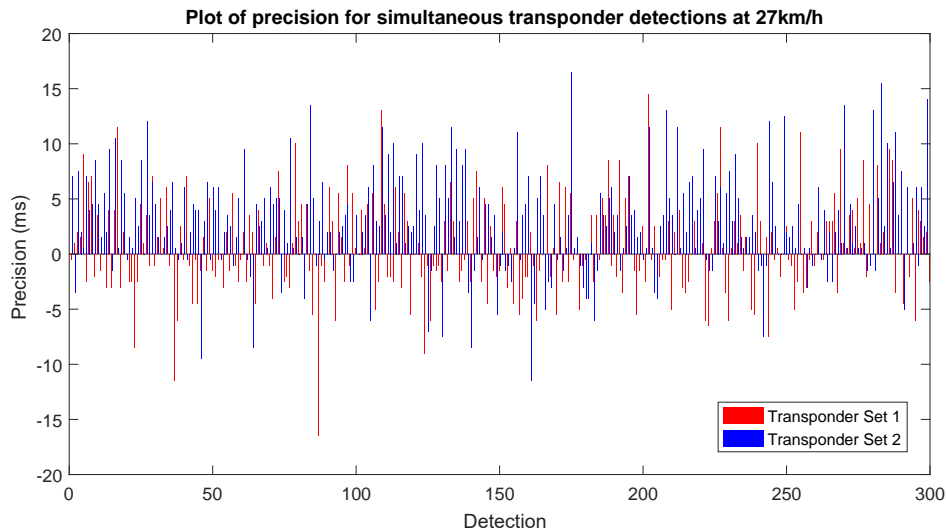


FIGURE 6.4: Test results showing precision of timing system generated using simultaneous transponder detections.

Figure 6.4 shows results for system precision based on the difference in recorded passing time of two sets of transponders, one attached to each end of the test apparatus armature. While Figure 6.4 shows that the majority of detections can be classified as precise to $\pm 10\text{ms}$, it also raises the question as to why the average

difference for transponder set one is 1ms and set two is 5ms, when it is expected that both should be 0ms. Although the 16MHz crystals specified in Appendix C have tolerances of 10ppm [47], the nRF51822 datasheet only specifies clock tolerances of 50ppm [35]. However, a crystal tolerance of 50ppm can only account for 500us of difference over 5s, the maximum time a transponder is permitted to calculate the centre sample. A further hypothesis is that supply voltage effects operating frequency, however results presented in Table 6.3 show this effect to be insignificant. Further testing is required to establish the cause of this offset.

| Device | Voltage | 5s Equivalent Time (s) |
|-------------|---------|------------------------|
| Decoder | 3.3V | 5.000845236 |
| Transponder | 3.3V | 5.000829611 |
| Transponder | 2.7V | 5.000835403 |

TABLE 6.3: Test results showing effect of supply voltage on operating frequency.

Results from an alternative method of measuring system precision are presented in Figure 6.5. This approach compares the detection times recorded to the SD card for a single transponder, against location reference data produced by the laser and LDR. To ensure correlation between the data recorded by the test apparatus and the times recorded by the decoder, a synchronising signal that toggles every second is output from the decoder and recorded by the test apparatus.

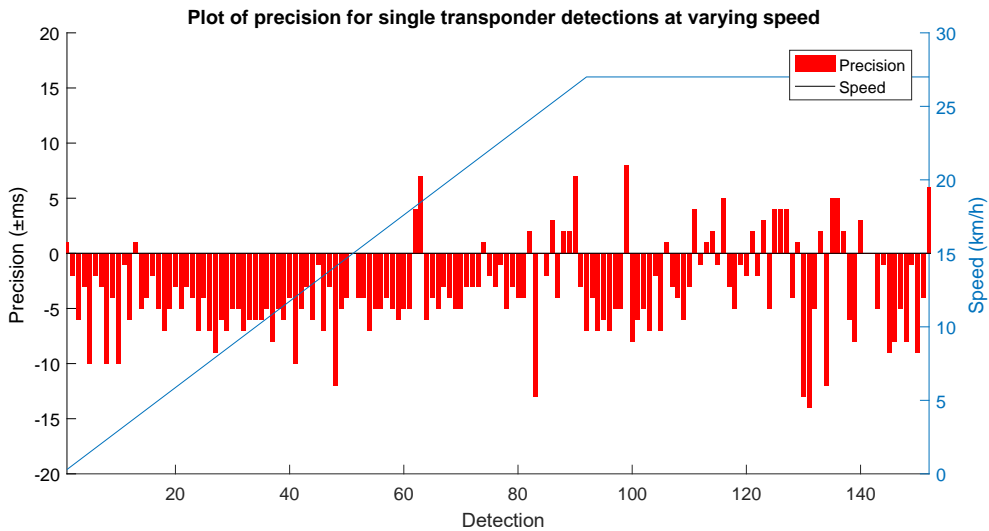


FIGURE 6.5: Test results showing precision of timing system generated using single transponder detections.

Precision values from Figure 6.5 produce an average precision of -3ms, with a negative precision meaning the detections preempted the actual centre crossing

time. This is not expected since only delays are present in the critical path. The precision appears to have only a minor relation to speed. It is therefore suggested the offset is consistent with data presented in Figure 6.4, however once again further work is required to determine the cause of the offset. Figure 6.6 provides evidence that the above test procedures produces consistent results, and also shows that greater than 90% of detections are precise to within $\pm 10\text{ms}$.

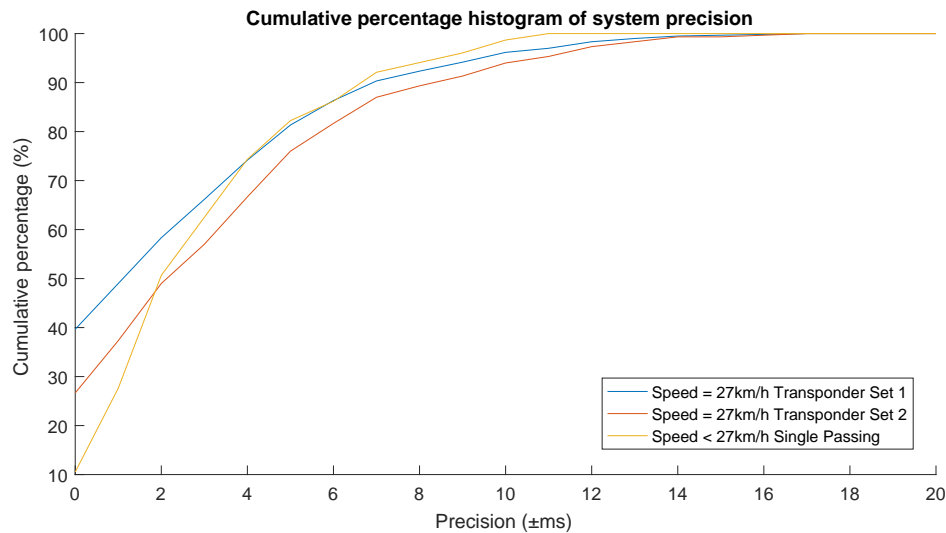


FIGURE 6.6: Histogram of system precision for various test methodologies.

Analysing the passing data presented in Figure 6.4 reveals a detection reliability of 99.7% (5 detections missed out of 1643 line crossings). However, it should be noted that for each missed detection, the corresponding transponder's wake counter was incremented, meaning the 2.4GHz transmission failed. Since the testing occurred in a built-up, urban environment, with lots of activity on the 2.4GHz frequency, it is suggested that the detection reliability may be higher when operated in the more remote locations used for club cycle racing. Further work is required to verify the validity of this result and improve upon it.

Further calculations based on the 50ppm system frequency tolerance discussed above reveal the decoder time-base to be accurate to within 180ms, over a one hour period. Combining this with the 3ms of average lead per detection reveals the system to be accurate enough for the purpose of timing club cycling races.

Results from a simulated race are presented below to verify the system's result generation capability. Table 6.4 shows the allocation of rider to transponder for the race.

| Bib# | FirstName | Tag |
|------|-----------|----------|
| 1 | JacobA | 23A4C561 |
| 2 | JacobB | 56F8B234 |
| 3 | JacobC | 29E7A514 |
| 4 | JacobD | 68B3E739 |

TABLE 6.4: Rider transponder allocation for test race.

Table 6.5 shows race data for JacobD transferred to CrossMgr via TCP. Entries where ‘Lap Time’ is ‘X’ are duplicated detections due to incorrect loop power setting and loop width, relative to detection height. This shows the system can still operate with an incorrect physical setup, important when operators are inexperienced. Comparing Table 6.5 to the full race file recorded to the SD card and presented in Appendix D, reveals SD card data matches TCP data. Although an adjustment is applied to account for mismatch between PC system clock and decoder clock.

| Lap | Lap Time | Race | Clock |
|-----|----------|-------|----------|
| 1 | 01:03 | 01:03 | 14:14:21 |
| 2 | 01:05 | 02:08 | 14:15:26 |
| 3 | 00:54 | 03:02 | 14:16:20 |
| 4 | 00:39 | 03:42 | 14:17:00 |
| | X | 03:42 | 14:17:00 |
| 5 | 01:24 | 05:06 | 14:18:24 |
| 6 | 00:58 | 06:04 | 14:19:21 |
| | X | 06:04 | 14:19:22 |
| 7 | 01:10 | 07:14 | 14:20:32 |
| 8 | 00:43 | 07:56 | 14:21:14 |
| 9 | 00:36 | 08:32 | 14:21:50 |
| 10 | 00:57 | 09:30 | 14:22:48 |

TABLE 6.5: Test race data for rider JacobD processed by CrossMgr.

| Pos | Bib | First Name | Time | Gap |
|-----|-----|------------|------|-------|
| 1 | 4 | JacobD | 9:30 | |
| 2 | 2 | JacobB | 9:34 | 0'05" |
| 3 | 3 | JacobC | 9:54 | 0'24" |
| 4 | 1 | JacobA | 9:54 | 0'24" |

TABLE 6.6: Test race results generated by CrossMgr.

Table 6.6 shows the final test race results corresponding to the data in Appendix D, while Figure 6.7 presents the corresponding graphical outputs produced by

CrossMgr. These include race playback and lap time breakdowns for all riders, as well as individual breakdowns plotted on a graph. Providing this data to riders encourages participation, increasing the popularity of the race or race series, making investment in the system more cost effective for clubs

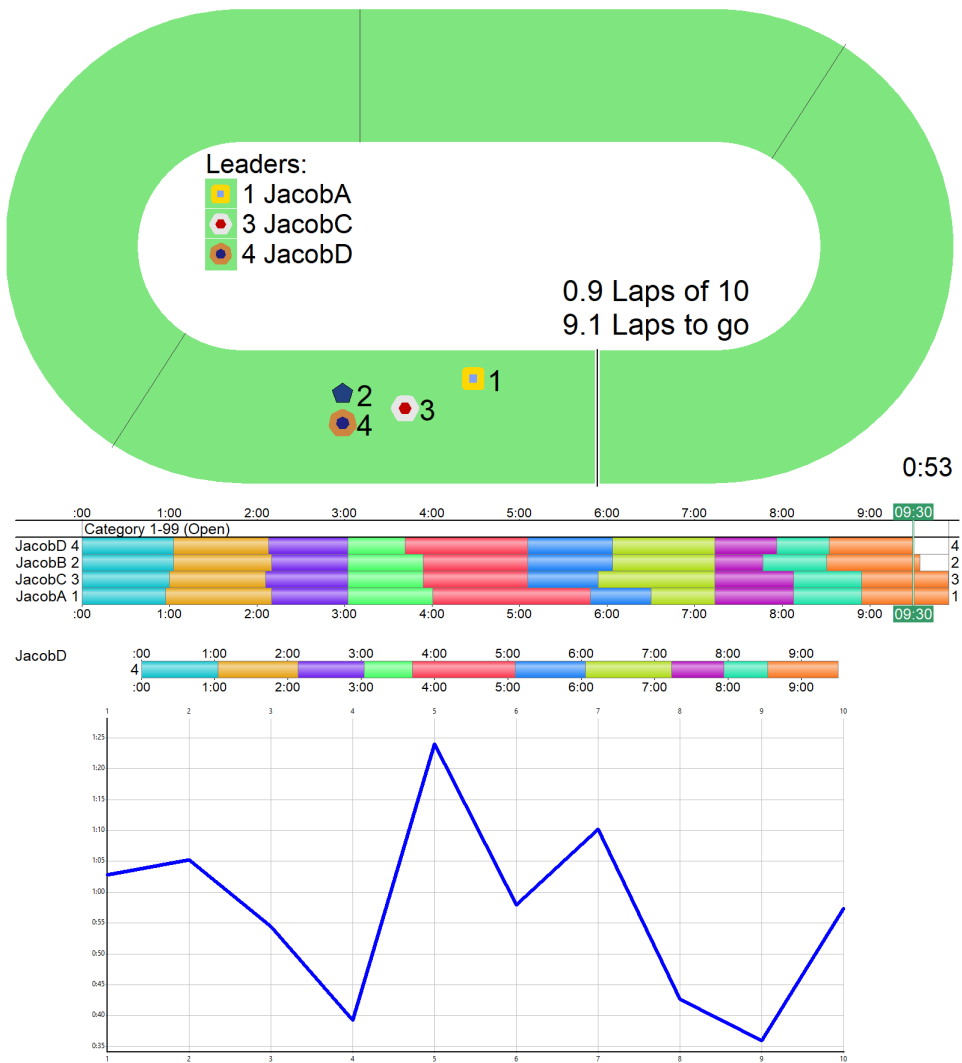


FIGURE 6.7: Example outputs from CrossMgr based on test race.

6.3 Commercial Viability

To assess the viability of the timing system developed in this project as a commercial product, a survey was publicised to cycling clubs in British Cycling's South-East region. Between questions, thirteen to seventeen responses were received.

The data shows that the participating cycling clubs organise between two and eighty races a year, and on average twenty. Participation in these races varies, with between five and four-hundred riders taking part, and on average one-hundred. While the specified rider limit of the system developed appears insufficient, it has not been possible to test the physical rider limit and so comparison to this data is not possible. Further work could enable a higher rider limit to be specified.

Out of the clubs organising races discussed above, only thirty-five percent of them use a fully automatic timing system to generate results. The following features where listed as making the existing systems suitable for timing club cycle races, quick generation of accurate results, the ability to run multiple races with multiple starts, transponders easily fixing to bikes, and an incorporated photo finish option. While it was suggested pricing, the requirement for a cable across the road, the requirement for mains power, complexity of operation and not being suitable for all types of racing made existing systems less suitable. The system developed in this project is able to maintain all of the advantages of the currently available systems, while addressing some of the disadvantages. None of the clubs using electronic timing systems owned the equipment, revealing a gap in the market for a system that clubs could afford to own.

The requirement for an affordable timing system is further justified by the ninety percent of the remaining clubs who have experienced barriers to being able to use an electronic timing system, with cost being the most prevalent. While further barriers were specified as lack of experience, lack of flexibility of software, poor reliability and insufficient precision. Although existing solution's precision is not improved upon, the system developed in this project makes progress in removing the other barriers. As discussed in Appendix A, the Project Brief, pen and paper combined with race footage is a popular method for manually recording results, although some clubs indicated that they use timing applications on a tablet as a semi-automatic solution. Lack of accuracy, being prone to errors, being time consuming, being challenging in low light, providing delayed results and requiring experienced volunteers were listed as disadvantages of these methods. This presents good reason for cycling clubs to use electronic timing systems for the generation of club cycle race results

When presented with the specification shown in Table 1.1 in Chapter 1, and asked if the system would be suitable for timing club cycling races, only three out of the fourteen respondents expressed concerns. These concerns included the rider limit and use of a loop of wire across a public road. While all clubs expressed

interest in owning the system, one club stated they do not provide extensive rider rankings as it is not encouraging for lower placed riders, therefore the system is not necessarily required. However, this opinion was not shared by other clubs, with the majority suggesting cost would be the definitive factor. Results show that the majority of clubs would expect transponders to be less than £10 each, while the decoder should be in the range of £250-£750. Since transponders cost roughly £8.75 to manufacture, running a profitable business whilst fulfilling this requirement would be challenging. Although, decoder manufacture costs would easily enable the suggested price range to be achieved. Therefore adjustment to the pricing scheme proposed in Section 6.1 is required.

Chapter 7

Conclusions

Figure E.2 and E.3 in Appendix E show Gantt charts of the proposed and actual schedule of work for the project respectively, while Figure E.1 presents the corresponding risk assessment. This enabled successful project completion by incorporating time management, risk awareness and contingency planning.

Tests of the resulting product show that a competitive timing system has been developed. Suitability for use in a cycling club environment is achieved through intuitive operation, fully waterproof construction, replaceable transponder batteries and the theoretical capability of recording races with up to one-hundred riders. While manufacturing costs of roughly £8.75 and £128.63 for the transponder and decoder respectively would enable the system to be sold at a significantly lower price than existing systems, survey data suggests that the transponder price reduction is not sufficient. A system precision exceeding $\pm 10\text{ms}$ for 90% of detections and a minimum observed reliability of 99.7% for detections provides a suitable but improvable timing performance.

Further work is proposed to improve timing performance by addressing the discrepancies in timing precision and reliability. Finalising the system design for manufacture is also required to ensure the prototype system can be mass produced to the same specifications. Since transponder design is considered as economical as possible, changes to the business model are required to reduce upfront cost of transponders to clubs. While further work is suggested, the current system design would enable cycling club races to be timed electronically, with many benefits over currently available systems.

Word Count of **9995** including main text body, titles, subtitles, excluding
tables/figures, table/figure labels, headers and footers.

Appendix A

Project Brief

Problem: Cycle racing is a unique sport because although riders are competing against one another they generally work together during the race. This race characteristic presents a challenge for recording results, as most riders will cross the finish line in quick succession. A common method used by clubs for recording races involves a pen and paper and often hours of volunteer time scrolling through video footage of the race. There are systems available for electronically recording times and positions of riders, however, the current market offerings are expensive to set-up and maintain, and complicated to operate.

Goal: The goal of this project is to design and build an electronic timing system specifically suited to the needs of cycling clubs that are organising races. To make the system suitable for club racing it will be:

- Easy to set-up, operate and produce results
- Designed for cost effective manufacturing
- High precision, high reliability but lower accuracy timing
- Capable of recording races with up to 100 riders
- Reusable transponders with minimal maintenance costs

Scope: For the purposes of this project, the system hardware will be the focus of development. An open-source cycling-specific timing software is already available and will be used for processing data generated by the hardware. The hardware will include two elements: transponders and a compatible decoder unit. The first step

will be developing a prototype transponder capable of detecting the start/finish line. Once this works reliably, a method for transmitting this data to the decoder box must be established. From here the design of the decoder circuit must be developed to include the detection circuitry as well as a user interface, power supply, PC interface and timer. Depending on progress, the complexity of the decoder unit may vary. The priority will be to transfer the transponder prototype to a PCB and if time allows, transfer the decoder prototype to a PCB also.

Appendix B

Example Cycling Venue Risk Assessment

Facility: SE136 Cyclopark 17-05-18

Standard Risk Assessment

Venue Name:

| |
|-----------|
| Cyclopark |
|-----------|

Venue ID:

| |
|-------|
| SE136 |
|-------|



Address:

| |
|---|
| The Tollgate, Wrotham Road, Gravesend, Kent |
|---|

Postcode:

| |
|----------|
| DA11 7NP |
|----------|

Description of facility:

Purpose built cycling facility. Full road circuit contains numerous cut through sections that can be used to create shorter circuits. Organisers of youth events should use a circuit that is suitable for the age categories participating

Summary

| | | | | | |
|--|--------------------------|-------------------|--------|-------------------|-----|
| Track Length: Full Circuit Flood Lit Circuit | 2.5 KM 1.1 KM | Track Surface: | Tarmac | Café | Yes |
| Track Width: | 6 Meters | Toilets / Showers | Yes | Car Park Capacity | 300 |

| Category | National | Regional | Youth |
|--|-----------|-----------|----------|
| Permissible Numbers (maximum): Full Circuit: Flood Lit Circuit: | 100 60 | 100 60 | 80 40 |

For National events, a separate application must be made to the National Events Team for an increase to the listed numbers

| | | |
|---------------|--------------|--|
| REO: | Mobile: | Email: |
| Simon Bedford | 07940 302253 | simonbedford@britishcycling.org.uk |
| RCA: | Mobile: | Email: |
| Eric Lejeune | 07852 167477 | bcsoutheastrca@gmail.com |

Local A&E Address:

| |
|--|
| Darent Valley Hospital Darent Wood Road, Dufford Kent, DA2 8DA |
|--|

Venue Owners / Operators:

| |
|---------------------------------------|
| Kent County Council / Cyclopark Trust |
|---------------------------------------|

Event Specific Details (to be completed in full):

Event Organiser (name, telephone):

| |
|--|
| |
|--|

Hosting Club:

| |
|--|
| |
|--|

Event Date:

| |
|--|
| |
|--|

First Aid Provider

| |
|--|
| |
|--|

Safety Measures

| | | |
|--|------------------------|----------|
| | Marshal with Red Flag | 4 |
| | 'Cycle Event' Sign | 2 |
| | Arrows - for direction | 0 |

| | | |
|--|----------|----------|
| | Padding | 0 |
| | Barriers | 6 |
| | | |

Risk Assessment:

Are all control measures in place:

Yes / No

| |
|--|
| |
|--|

If No, have changes been recorded on Dynamic Risk Assessment:

Yes / No

| |
|--|
| |
|--|

Please return this page and the Dynamic Risk Assessment with your Commissaires Report.

FIGURE B.1: Risk assessment for cycling facility often used for club cycling races [9].

Appendix C

Bill of Materials

| Qty | Value | Package | Parts | Description | Manufacturer | Unit Pric | Total Price |
|-----|---------------------|-----------|------------------------|---------------------|--------------|--------------|-------------|
| 1 | 112 | CR2032 | B1 | Battery Contact | Keystone | £0.08 | £0.08 |
| 1 | 110 | CR2032 | B1 | Battery Contact | Keystone | £0.11 | £0.11 |
| 1 | 0.8pF | C0402 | C8 | Capacitor | | £0.01* | £0.01 |
| 1 | 1.5pF | C0402 | C9 | Capacitor | | £0.01* | £0.01 |
| 7 | 100nF | C0402 | C2,C3,C4,C5,C6,C10,C11 | Capacitor | | £0.01* | £0.07 |
| 4 | 12pF | C0402 | C12,C13,C14,C15 | Capacitor | | £0.01 | £0.04 |
| 1 | 2.2pF | C0402 | C7 | Capacitor | | £0.01* | £0.01 |
| 1 | 680pF | C0402 | C1 | Capacitor | | £0.01* | £0.01 |
| 1 | X1E000021011612 | 3.2X2.5mm | Y2 | Crystal (16MHz) | Epson | £0.31 | £0.31 |
| 1 | ABS07-32.768KHZ-1-T | 3.2X1.5mm | Y1 | Crystal (32.768kHz) | ABRACON | £0.49 | £0.49 |
| 1 | 2.38mH | 4513TC | L1 | Inductor | Coilcraft | £0.99 | £0.99 |
| 1 | 10nH | L0402 | L3 | Inductor | | £0.01* | £0.01 |
| 1 | 3.3nH | L0402 | L4 | Inductor | | £0.01* | £0.01 |
| 1 | 4.7nH | L0402 | L2 | Inductor | | £0.01* | £0.01 |
| 1 | AS3930 | QFN16 | IC2 | LF Wakeup IC | AMS | £1.56 | £1.56 |
| 1 | 1K | R0402 | R1 | Resistor | | £0.01* | £0.01 |
| 1 | 12K | R0402 | R2 | Resistor | | £0.01* | £0.01 |
| 1 | NRF51822QFAC | QFN40 | IC1 | RF SOC | Nordic | £1.76 | £1.76 |
| 1 | Case | | | | | £0.10 | £0.10 |
| 1 | PCB | | | | JLC PCB | £0.01 | £0.01 |
| 1 | CR2032 | | | | Panasonic | £0.23 | £0.23 |
| 29 | Assembly | | | | | £0.05 | £1.45 |
| | | | | | Total | £7.29 | |

Table C.1: Estimated BOM for transponder assembly.

| Qty | Value | Package | Parts | Description | Manufacturer | Unit Price | Total Price |
|-----|-----------------|-----------|---|--------------------|--------------|------------|-------------|
| 1 | MCP73213 | DFN10 | IC4 | Battery Charger IC | Microchip | £1.04 | £1.04 |
| 1 | TPS62153 | QFN25_3X3 | IC5 | Buck Regulator IC | Texas Inst. | £0.70 | £0.70 |
| 1 | ABI-042-RC | 12mm | LS1 | Buzzer | Pro Signal | £1.39 | £1.39 |
| 1 | 0.8pF | C0603 | C8 | Capacitor | | £0.01* | £0.01 |
| 1 | 1.5pF | C0603 | C9 | Capacitor | | £0.01* | £0.01 |
| 16 | 100nF | C0603 | C3,C4,C5,C6,C10,C11, C16,C32,C33,C19,C39, C40,C41,C42,C43,C45 | Capacitor | | £0.01* | £0.16 |
| 5 | 10nF | C0603 | C20,C27,C28,C36,C46 | Capacitor | | £0.01* | £0.05 |
| 2 | 10pF | C0603 | C17,C18 | Capacitor | | £0.01* | £0.02 |
| 2 | 10uF | C0603 | C23,C24 | Capacitor | | £0.01* | £0.02 |
| 4 | 12pF | C0603 | C12,C13,C14,C15 | Capacitor | | £0.01* | £0.04 |
| 1 | 2.2pF | C0603 | C7 | Capacitor | | £0.01* | £0.01 |
| 1 | 22nF | C0603 | C31 | Capacitor | | £0.01* | £0.01 |
| 1 | 3.3nF | C0603 | C30 | Capacitor | | £0.01* | £0.01 |
| 1 | 4.7uF | C0603 | C22 | Capacitor | | £0.01* | £0.01 |
| 2 | 10uF | C0805 | C29,C44 | Capacitor | | £0.01* | £0.02 |
| 5 | 22uF | C0805 | C21,C25,C26,C34,C38 | Capacitor | | £0.01* | £0.05 |
| 1 | ECHU1H154GX9 | ECHU1HD | C2 | Capacitor (150nF) | Panasonic | 0.435 | £0.44 |
| 1 | ECHU1H224GX9 | ECHU1HD | C1 | Capacitor (220nF) | Panasonic | 0.614 | £0.61 |
| 1 | 61301421821 | 2X7 | J5 | Connector | Wurth Elec. | £0.34 | £0.34 |
| 1 | 61301421021 | 2X7_RA | J6 | Connector | Wurth Elec. | £0.37 | £0.37 |
| 1 | 448382 | DCJACK | CN1 | Connector | RS PRO | £0.54 | £0.54 |
| 1 | JST-PH-2-SMT-RA | JST | CN2 | Connector | JST | £0.25 | £0.25 |

| | | | | | | | |
|---|--------------------------------|-----------|---------------------|---------------------|-------------|--------|-------|
| 1 | 693071010811 | MICROSD | CN4 | Connector | Wurth Elec. | £1.39 | £1.39 |
| 2 | SSW-108-04-G-S | 1X8 | U1 | Connector | Samtec | £0.63 | £1.26 |
| 1 | 7499010211A | RJ45 | CN3 | Connector | Wurth Elec. | £5.19 | £5.19 |
| 1 | U.FL-R-SMT(01) | U.FL | X1 | Connector | Hirose | £0.44 | £0.44 |
| 1 | X1E000021011612 | 3.2X1.5mm | Q1 | Crystal (16MHz) | Epson | £0.31 | £0.31 |
| 1 | RH100-25.000-18-F-303 0-EXT | 3.2X1.5mm | Y1 | Crystal (25MHz) | Raltron | £0.64 | £0.64 |
| 1 | ABS07-32.768KHZ-1-T | 3.2X1.5mm | Q2 | Crystal (32.768kHz) | ABRACON | £0.49 | £0.49 |
| 1 | MCP45HV | QFN25 | IC3 | Digital Pot IC | Microchip | £0.88 | £0.88 |
| 2 | CD214A-B340LF | SMA | D2,D3 | Diode | Bourns | 0.122 | £0.24 |
| 1 | MBR120VLSFT3G | SOD-123 | D1 | Diode | ON Semi. | £0.07 | £0.07 |
| 1 | W5500 | TQFP48 | IC2 | Ethernet Controller | Wiznet | £1.28 | £1.28 |
| 1 | 74279206 | L0805 | L12 | Ferrite Bead (30R) | Wurth Elec. | £0.01* | £0.01 |
| 1 | 10nH | L0603 | L3 | Inductor | | £0.01* | £0.01 |
| 1 | 3.3nH | L0603 | L4 | Inductor | | £0.01* | £0.01 |
| 1 | 4.7nH | L0603 | L2 | Inductor | | £0.01* | £0.01 |
| 1 | MSS1278-154KLD | 12X12mm | L1 | Inductor (150uH) | Coilcraft | £0.73 | £0.73 |
| 1 | SPX3819M5_3_3 | SOT23-5 | IC6 | LDO Regulator | Exar | £0.17 | £0.17 |
| 2 | RED | LED5mm | LED1,LED2 | LED | | £0.04 | £0.09 |
| 1 | 12uH | 5X5mm | L5 | LPS5030-123MRB | Coilcraft | 0.468 | £0.47 |
| 1 | 3.3uH | 5X5mm | L7 | LPS5030-332MRB | Coilcraft | £0.55 | £0.55 |
| 1 | IPD80R1K4P7ATMA1 | DPAK | Q3 | MOSFET | Infineon | £0.38 | £0.38 |
| 2 | IRLML0030TRPBF | SOT23-3 | Q4,Q5 | MOSFET | Infineon | 0.07 | £0.14 |
| 5 | 10K | CAY16 | RN1,RN3,RN4,RN8,RN9 | Resistor | | £0.01* | £0.05 |
| 1 | 1K6 | R0603 | R3 | Resistor | | £0.01* | £0.01 |
| 3 | 100K | R0603 | R11,R12,R26 | Resistor | | £0.01* | £0.03 |
| 2 | 33K | R0603 | R25,R27 | Resistor | | £0.01* | £0.02 |

| | | | | | | | |
|---|------------------------------|----------|-----------------|-------------------|-------------|--------|--------|
| 3 | 10K | R0603 | R4,R7,R16 | Resistor | | £0.01* | £0.03 |
| 1 | 91R | R0603 | R19 | Resistor | | £0.01* | £0.01 |
| 1 | 10R | R0603 | R24 | Resistor | | £0.01* | £0.01 |
| 1 | 12K | R0603 | R2 | Resistor | | £0.01* | £0.01 |
| 1 | 12k4-1% | R0603 | R8 | Resistor | | £0.01* | £0.01 |
| 1 | 130R | R0603 | R18 | Resistor | | £0.01* | £0.01 |
| 3 | 1K | R0603 | R15,R20,R21 | Resistor | | £0.01* | £0.03 |
| 1 | 20R | R0603 | R17 | Resistor | | £0.01* | £0.01 |
| 2 | 390R | R0603 | R5,R6 | Resistor | | £0.01* | £0.02 |
| 4 | 49R9 | R0603 | R9,R10,R22,R23 | Resistor | | £0.01* | £0.04 |
| 2 | 4K7 | R0603 | R13,R14 | Resistor | | £0.01* | £0.02 |
| 1 | 352110RFT | R2512 | R1 | Resistor (10R) | TE Conn. | 0.186 | £0.19 |
| 1 | NRF51822QFAC | QFN40 | IC1 | RF SOC | Nordic | £1.76 | £1.76 |
| 2 | 7466313 | WP-SMT | E1,E2 | Right Angle Mount | Wurth Elec. | 1.75 | £3.50 |
| 4 | 3550 | 3550 | J1,J2,SW5 | Spade Socket | Keystone | £0.18 | £0.70 |
| 4 | 431256083716 | 6X6_TACT | SW1,SW2,SW3,SW4 | Tactile Switch | Wurth Elec. | £0.24 | £0.96 |
| 1 | TC33X-2-103E | TC33X | TM1 | Trimmer Pot | Bourns | 0.093 | £0.09 |
| 1 | 96023134 | | | Case | Bocube | £18.35 | £18.35 |
| 4 | 96708000 | | | M3 Standoff | Bocube | £0.25 | £1.00 |
| 4 | 971250321 | | | 25mm M3 Standoff | Wurth Elec. | £0.25 | £0.98 |
| 4 | M3 Bolt | | | | | £0.01* | £0.04 |
| 2 | 972 355-101 | | | Banana Jack | Hirschmann | £1.48 | £2.96 |
| 2 | 53102001 | | | O-Ring | Lapp Kabel | £0.02 | £0.04 |
| 1 | R-132G7210100CC | | | SMA Assembly | Multicomp | £5.62 | £5.62 |
| 1 | 471001264143 | | | Rocker Switch | Wurth Elec. | £2.00 | £2.00 |
| 1 | NHD-0420H1Z-FSW-G BW-33V3 | | | LCD | NewHaven | £10.30 | £10.30 |

| | | | | | | | |
|-----|--------------------|--|--|------------------|-----------|--------------|----------------|
| 2 | ASB-2020E | | | 20mm M2 standoff | Hirosugi | £0.50 | £1.00 |
| 4 | M2 Bolt | | | | | £0.01* | £0.05 |
| 1 | 7.4V 2600mAh | | | LiIon Battery | RS Pro | £16.30 | £16.30 |
| 1 | FBKR35068-SM-KR | | | Whip Antenna | EAD | £6.23 | £6.23 |
| 1 | PHR-2 | | | JST housing | JST | £0.02 | £0.02 |
| 2 | BPH-002T-P0.5S | | | JST Crimps | JST | £0.02 | £0.03 |
| 2 | LED3-22 | | | LED Spacer | Multicomp | £0.05 | £0.09 |
| 1 | Waterproof Buttons | | | | | £2.00 | £5.00 |
| 1 | PCB | | | | JLC PCB | £1.00 | £1.00 |
| 156 | Assembly | | | | | £0.05 | £7.80 |
| | | | | | | Total | £104.19 |

Table C.2: Estimated BOM for decoder assembly.

*Pricing estimate for common low cost component.

Assembly cost estimated at 5p per component. Injection Moulding (case/water-proof buttons) cost estimated. All other pricing based on distributor max price break. All prices exclude VAT.

Appendix D

Test Race Data

| Test Race Passing Data |
|--|
| 01;23A4C561;2019-03-20;14:13:26.069;0;0058;13;0;1;1;2;0;109;2.89;12;0;c327af89 02;29E7A514;2019-03-20;14:13:26.073;0;0061;13;0;1;1;2;0;070;2.93;12;0;c327af89 03;68B3E739;2019-03-20;14:13:26.071;0;0066;13;0;1;1;2;0;168;2.85;12;0;c327af89 04;56F8B234;2019-03-20;14:13:26.072;0;0076;13;0;1;1;2;0;078;2.88;12;0;c327af89 05;23A4C561;2019-03-20;14:14:15.331;0;0107;12;0;1;1;2;0;110;2.89;12;0;c327af89 06;29E7A514;2019-03-20;14:14:17.954;0;0045;12;0;1;1;2;0;071;2.93;12;0;c327af89 07;68B3E739;2019-03-20;14:14:20.554;0;0052;13;0;1;1;2;0;169;2.86;12;0;c327af89 08;56F8B234;2019-03-20;14:14:20.555;0;0083;13;0;1;1;2;0;079;2.88;12;0;c327af89 09;29E7A514;2019-03-20;14:15:23.600;0;0047;11;0;1;1;2;0;072;2.93;12;0;c327af89 10;68B3E739;2019-03-20;14:15:25.763;0;0049;10;0;1;1;2;0;170;2.85;12;0;c327af89 11;23A4C561;2019-03-20;14:15:27.677;0;0108;12;0;1;1;2;0;111;2.89;13;0;c327af89 12;23A4C561;2019-03-20;14:15:27.675;0;0108;12;0;1;1;2;0;111;2.89;13;1;c327af89 13;56F8B234;2019-03-20;14:15:27.677;0;0122;13;0;1;1;2;0;080;2.88;12;1;c327af89 14;23A4C561;2019-03-20;14:16:20.099;0;0024;02;0;1;1;2;0;112;2.90;13;0;c327af89 15;56F8B234;2019-03-20;14:16:20.093;0;0031;03;0;1;1;2;0;081;2.88;12;0;c327af89 16;29E7A514;2019-03-20;14:16:20.175;0;0092;14;0;1;1;2;0;073;2.93;13;0;c327af89 17;68B3E739;2019-03-20;14:16:20.174;0;0097;13;0;1;1;2;0;171;2.86;13;0;c327af89 18;23A4C561;2019-03-20;14:16:20.400;0;0009;00;0;1;1;2;0;113;2.88;13;0;c327af89 19;56F8B234;2019-03-20;14:16:20.410;0;0009;00;0;1;1;2;0;082;2.87;12;0;c327af89 20;68B3E739;2019-03-20;14:16:59.444;0;0027;02;0;1;1;2;0;172;2.86;13;0;c327af89 21;68B3E739;2019-03-20;14:16:59.752;0;0009;00;0;1;1;2;0;173;2.85;13;0;c327af89 22;29E7A514;2019-03-20;14:17:11.912;0;0084;13;0;1;1;2;0;074;2.93;13;0;c327af89 23;56F8B234;2019-03-20;14:17:11.915;0;0101;13;0;1;1;2;0;083;2.88;12;0;c327af89 24;23A4C561;2019-03-20;14:17:18.376;0;0043;03;0;1;1;2;0;114;2.89;13;0;c327af89 25;23A4C561;2019-03-20;14:17:18.697;0;0009;00;0;1;1;2;0;115;2.88;13;0;c327af89 26;29E7A514;2019-03-20;14:18:23.484;0;0127;16;0;1;1;2;0;075;2.93;13;0;c327af89 27;68B3E739;2019-03-20;14:18:23.487;0;0124;15;0;1;1;2;0;174;2.85;13;0;c327af89 28;56F8B234;2019-03-20;14:18:23.488;0;0191;16;0;1;1;2;0;084;2.87;13;0;c327af89 29;23A4C561;2019-03-20;14:19:06.243;0;0021;02;0;1;1;2;0;116;2.90;13;0;c327af89 30;23A4C561;2019-03-20;14:19:06.544;0;0009;00;0;1;1;2;0;117;2.88;13;0;c327af89 |

| |
|--|
| 31;29E7A514;2019-03-20;14:19:11.687;0;0047;13;0;1;1;2;0;076;2.93;13;0;c327af89 |
| 32;68B3E739;2019-03-20;14:19:21.374;0;0027;03;0;1;1;2;0;175;2.86;13;0;c327af89 |
| 33;56F8B234;2019-03-20;14:19:21.429;0;0114;14;0;1;1;2;0;085;2.88;13;0;c327af89 |
| 34;68B3E739;2019-03-20;14:19:21.685;0;0009;00;0;1;1;2;0;176;2.85;13;0;c327af89 |
| 35;23A4C561;2019-03-20;14:19:47.792;0;0100;15;0;1;1;2;0;118;2.89;13;0;c327af89 |
| 36;29E7A514;2019-03-20;14:20:31.478;0;0049;03;0;1;1;2;0;077;2.93;13;0;c327af89 |
| 37;23A4C561;2019-03-20;14:20:31.477;0;0053;03;0;1;1;2;0;119;2.89;13;0;c327af89 |
| 38;56F8B234;2019-03-20;14:20:31.483;0;0088;03;0;1;1;2;0;086;2.88;13;0;c327af89 |
| 39;68B3E739;2019-03-20;14:20:31.613;0;0128;16;0;1;1;2;0;177;2.85;13;0;c327af89 |
| 40;29E7A514;2019-03-20;14:20:31.817;0;0032;01;0;1;1;2;0;078;2.93;13;0;c327af89 |
| 41;23A4C561;2019-03-20;14:20:31.833;0;0025;01;0;1;1;2;0;120;2.89;13;0;c327af89 |
| 42;56F8B234;2019-03-20;14:20:31.866;0;0009;00;0;1;1;2;0;087;2.87;13;0;c327af89 |
| 43;56F8B234;2019-03-20;14:21:04.465;0;0107;13;0;1;1;2;0;088;2.88;13;0;c327af89 |
| 44;68B3E739;2019-03-20;14:21:14.227;0;0057;13;0;1;1;2;0;178;2.86;13;0;c327af89 |
| 45;29E7A514;2019-03-20;14:21:25.566;0;0015;01;0;1;1;2;0;079;2.94;13;0;c327af89 |
| 46;29E7A514;2019-03-20;14:21:25.862;0;0009;00;0;1;1;2;0;080;2.93;13;0;c327af89 |
| 47;23A4C561;2019-03-20;14:21:25.632;0;0175;16;0;1;1;2;0;121;2.88;13;1;c327af89 |
| 48;56F8B234;2019-03-20;14:21:48.179;0;0141;13;0;1;1;2;0;089;2.88;13;0;c327af89 |
| 49;68B3E739;2019-03-20;14:21:50.169;0;0124;15;0;1;1;2;0;179;2.86;13;0;c327af89 |
| 50;29E7A514;2019-03-20;14:22:12.202;0;0074;14;0;1;1;2;0;081;2.93;13;0;c327af89 |
| 51;23A4C561;2019-03-20;14:22:12.185;0;0137;13;0;1;1;2;0;122;2.89;13;0;c327af89 |
| 52;68B3E739;2019-03-20;14:22:47.526;0;0107;13;0;1;1;2;0;180;2.86;13;0;c327af89 |
| 53;56F8B234;2019-03-20;14:22:52.052;0;0057;02;0;1;1;2;0;090;2.88;13;0;c327af89 |
| 54;56F8B234;2019-03-20;14:22:52.390;0;0009;00;0;1;1;2;0;091;2.87;13;0;c327af89 |
| 55;29E7A514;2019-03-20;14:23:11.697;0;0023;02;0;1;1;2;0;082;2.94;13;0;c327af89 |
| 56;29E7A514;2019-03-20;14:23:11.998;0;0009;00;0;1;1;2;0;083;2.93;13;0;c327af89 |
| 57;23A4C561;2019-03-20;14:23:11.790;0;0224;15;0;1;1;2;0;123;2.88;13;0;c327af89 |

Table D.1: Test race passing data stored on SD card.

Appendix E

Project Management

| Potential Risk | Risk likeliness | Risk severity | Risk avoidance |
|--|-------------------|---------------|---|
| Cannot detect start/finish line using RF | Unlikely | Very high | Test the concept early in development allowing time for an alternative solution to be found. |
| Component failure | Possible | Medium | Build redundancy into time plan and use components that are readily available. |
| PCB manufacturing delay | Possible | High | Allow plenty of time for PCB assembly which can be used as contingency for delayed PCB. |
| Unable to source components | Unlikely/possible | Medium | Choose parts made by multiple manufacturers and/or ensure good stock levels and component lifetime plans. |
| PCB design includes fault | Likely | Medium/High | Prototype the entire circuit before PCB manufacture and allow extra time for new PCBs to be made. |
| Data loss | Unlikely | Very high | Keep multiple local copies as well as cloud based copies with version control features. |
| Componet misunderstanding | Possible | Medium | Test components thoroughly before committing them to the PCB design. |
| Ethernet doesn't work | Possible | Medium | Use serial to TCP bridge on host and send data over serial port from decoder |

FIGURE E.1: Table showing risk analysis.

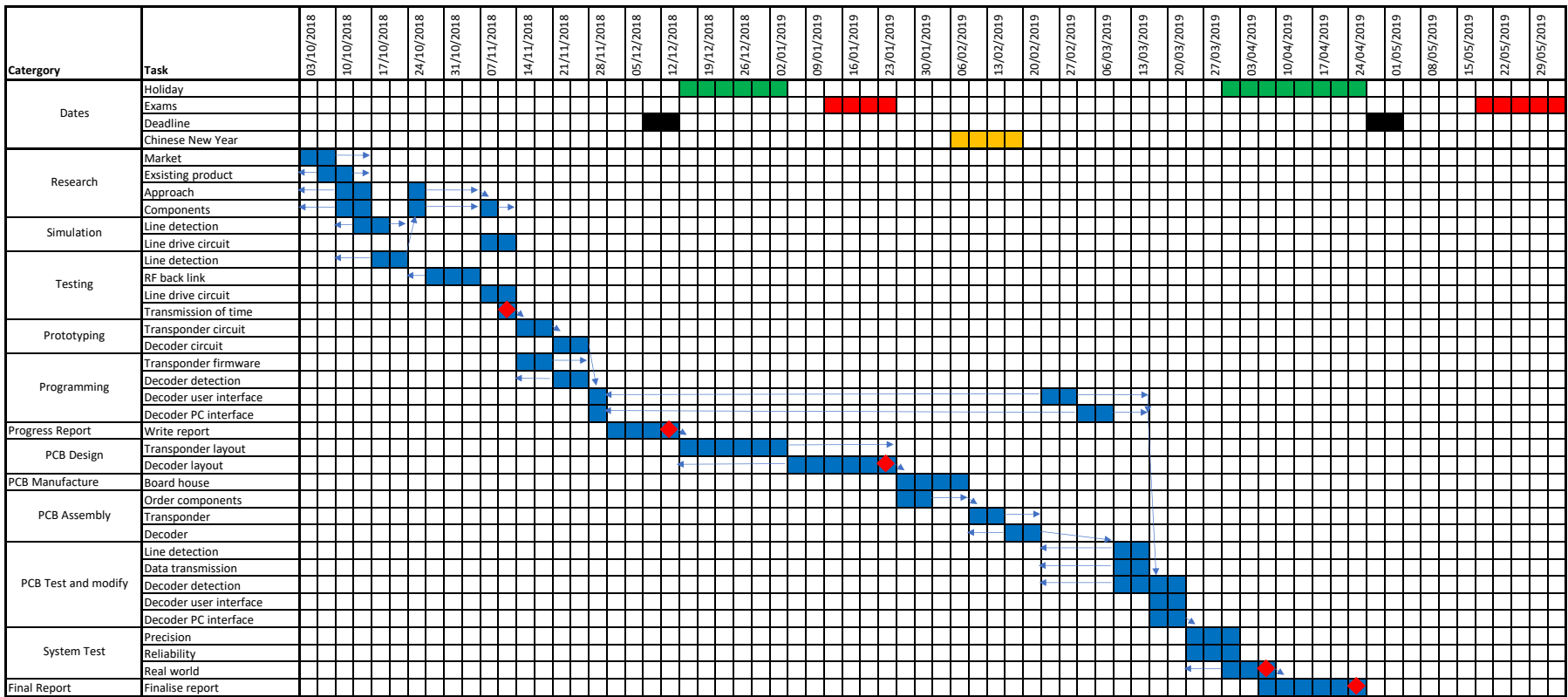


FIGURE E.2: Gantt chart of proposed work.

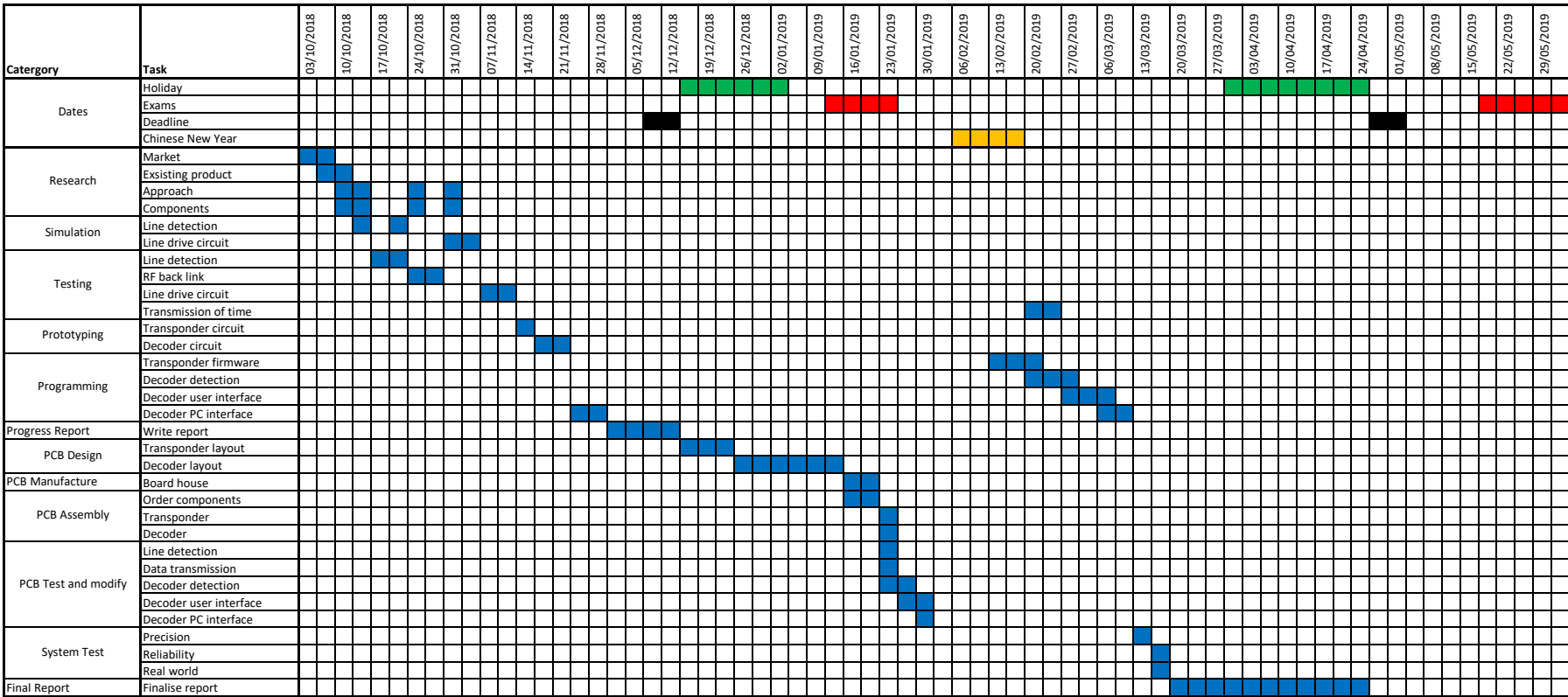


FIGURE E.3: Gantt chart of work completed.

Appendix F

Design Archive

The provided design archive is organised in the following way. All necessary project files are included.

Ethics

Ethics application for product viability survey.

Figures

All Figures included in final report.

Hardware

Decoder PCB and CAD files.

Transponder PCB and CAD files.

Supporting documentation and libraries.

Management

Gantt chart and risk management documentation.

Simulation

Acceleration error simulation files.

Class-E amplifier simulation files.

Start/finish line field simulation files.

Software

Make compilable transponder software.

Make compilable decoder software.

Testing

AS3930 test files.

Crystal tolerance test files.

MATLAB plotter file.

Precision and reliability test files.

Survey results.

TCP test files.

Test race files.

Bibliography

- [1] D. Hunt, A. Puglia, and M. Puglia, *RFID: a guide to radio frequency identification*. Wiley, 2007.
- [2] J. Pessinger, “Internal photos,” *FCC ID: 2832392 Application ID: EFU46nG0rsurYLYVQf0Jsg==*, Nov. 2015.
- [3] Vandermr, “Internal photos,” *FCC ID: 1191746 Application ID: F5lvZd/kjPXxK+IZl4Jn0A==*, Nov. 2009.
- [4] R. Correia and N. B. Carvalho, “Ultrafast backscatter modulator with low-power consumption and wireless power transmission capabilities,” *IEEE*, Oct. 2017.
- [5] Waveshare. (2016) Core51822. [Online]. Available: <https://www.waveshare.com/w/upload/5/57/Core51822-Schematic.pdf>
- [6] Arduino. (2018) Arduino mkr eth shield. [Online]. Available: <https://store.arduino.cc/arduino-mkr-eth-shield>
- [7] BOPLA. (2019) Bocube. [Online]. Available: <https://www.bopla.de/en/enclosure-technology/product/bocube.html>
- [8] Avtanski. (2019) Lcd display screenshot generator. [Online]. Available: <http://avtanski.net/projects/lcd/>
- [9] British Cycling, “Standard risk assessment,” *Facility: SE136 Cyclopark*, May 2018.
- [10] RFID4U. (2018) How to select a correct tag frequency. [Online]. Available: <https://rfid4u.com/rfid-basics-resources/how-to-select-a-correct-tag-frequency/>
- [11] Digikey. (2019) Battery life calculator. [Online]. Available: <https://www.digikey.co.uk/en/resources/conversion-calculators/conversion-calculator-battery-life>

- [12] RS PRO, “Article: 1449410,” *RS Pro 18650 Datasheet*, 2019.
- [13] Panasonic, “Cr2032,” *Manganese Dioxide Lithium Batteries Datasheet*, 2006.
- [14] British Cycling. (2016) British cycling reaches 125,000 members milestone. [Online]. Available: <https://www.britishcycling.org.uk>
- [15] R. Race Timing Systems. (2017) Joey timing system. [Online]. Available: <https://rfidtiming.com/product-details/joey-timing-system/>
- [16] MYLAPS. (2018) Prochip system. [Online]. Available: <https://www.mylaps.com/systems/prochip-system/>
- [17] Race Result AG, “Race result system,” *Active Transponders/USB Timing Box datasheet*, 2018.
- [18] TAGHeuer. (2018) Road cycling solution - race timing systems. [Online]. Available: <http://www.tagheuer-timing.com/en/race-timing-systems-cycling-road-cycling>
- [19] M. Venturini. (2018) Rchourglass. [Online]. Available: <https://github.com/mv4wd/RCHourglass>
- [20] MYLAPS. (2018) Rc4 timing system. [Online]. Available: <https://www.mylaps.com/systems/rc-4-timing-system/>
- [21] MOTOSPONDER. (2018) Hi-performance is at the heart of it! [Online]. Available: <http://www.motosponder.com/>
- [22] SIMPLIFASTER. (2018) Freelap fxchip. [Online]. Available: <https://store.simplifaster.com/freelap-fxchip>
- [23] LapSnapper. (2018) Lapsnapper lap timing system for karting. [Online]. Available: <https://www.lapsnapper.com/shop/lapsnapper-lap-timing-system-for-karting/>
- [24] S. Zuffanelli, “Antenna design solutions for rfid tags based on metamaterial inspired resonators and other resonant structures,” Ph.D. dissertation, Dept. Elect. Eng., UAB, Barcelona, 2016.
- [25] Race Result AG. (2018) Knowledge base, developers. [Online]. Available: <https://www.raceresult.com/en/support/kb.php?id=2791-Developers>
- [26] Y. He, “Study of magnetic field coupling technologies in activating rfid-sim card mobile payments,” *Springer*, Sep. 2012.

- [27] Y. Lee, “Antenna circuit design for rfid applications,” *Microchip AN710*, 2003.
- [28] Q. Kang, Z. Xie, Y. Liu, and M. Zhou, “125khz wake-up receiver and 433mhz data transmitter for battery-less tpms,” *IEEE*, Oct. 2017.
- [29] AMS, “3d low frequency wakeup receiver datasheet,” *AS3932 datasheet*, Mar. 2015.
- [30] B. Bai, X. Zhu, H. Zhang, and Z. Zhang, “Active rfid tags for smart shelf based on lf assistant devices,” *Springer*, Aug. 2017.
- [31] Coilcraft, “Rfid transponder coil,” *4513TC datasheet*, Oct. 2008.
- [32] D. G. Wilson, *Bicycling Science*. MIT Press, 2004.
- [33] S. Shi, T. Lu, H. Zhang, L. Xu, and T. A. Gulliver, “A design of active rfid tags based on nrf24l01,” *IEEE*, Dec. 2013.
- [34] Wangbo, “The wireless data transmission system design based on nrf2401,” *IEEE*, May 2009.
- [35] Nordic Semiconductor, “Multiprotocol bluetooth low energy/2.4 ghz rf system on chip,” *nRF51822 Product Specification v3.3*, 2014.
- [36] R. Lourens, “Low-frequency magnetic transmitter design,” *Microchip AN232*, 2008.
- [37] J. B. Hagen, *Radio-Frequency Electronics Circuits and Applications*. 2nd ed. Cambridge, New York: Cambridge University Press, Jun. 2009.
- [38] Microchip, “Ds20005304a,” *MCP45HDX1 datasheet*, Mar. 2014.
- [39] WIZnet Co., “Version 1.0.4,” *W5500 datasheet*, Oct. 2013.
- [40] Microchip, “Ds20002190c,” *MCP73213 datasheet*, Mar. 2014.
- [41] TAKACHI. (2017) Plastic enclosures. [Online]. Available: http://www.takachi-enclosure.com/data/p_01plastic.html
- [42] OKW. (2019) Plastic enclosures. [Online]. Available: <https://www.okw.com/en/Products/Plastic-enclosures.htm>
- [43] H. MANUFACTURING.

-
- [44] Kristin. (2015) General pcb design guidelines for nrf51. [Online]. Available: <https://devzone.nordicsemi.com/b/blog/posts/general-pcb-design-guidelines-for-nrf51>
 - [45] Nordic Semiconductor, “l/4 printed monopole antenna for 2.45ghz,” *White Paper*, Jan. 2005.
 - [46] International Electrotechnical Commission, “60529 standard,” *International Protection Marking*, 2019.
 - [47] Seiko Epson, “Tsx-3225,” *Crystal Unit Datasheet*, 2019.